The Growth Mechanisms of Macroscopic Bodies in Protoplanetary Disks

Jürgen Blum[1] and Gerhard Wurm[2]

[1]Institut für Geophysik und Extraterrestrische Physik, Technische Universität zu Braunschweig, Germany; email: j.blum@tu-bs.de

[2]Institut für Planetologie, Westfälische-Wilhelms-Universität Münster, Germany; email: gwurm@uni-muenster.de

Key Words

dust growth, laboratory astrophysics, origin of solar system, planet formation, planetesimals, protoplanetary dust

Abstract

The formation of planetesimals, the kilometer-sized planetary precursors, is still a puzzling process. Considerable progress has been made over the past years in the physical description of the first stages of planetesimal formation, owing to extensive laboratory work. This review examines the experimental achievements and puts them into the context of the dust processes in protoplanetary disks. It has become clear that planetesimal formation starts with the growth of fractal dust aggregates, followed by compaction processes. As the dust-aggregate sizes increase, the mean collision velocity also increases, leading to the stalling of the growth and possibly to fragmentation, once the dust aggregates have reached decimeter sizes. A multitude of hypotheses for the further growth have been proposed, such as very sticky materials, secondary collision processes, enhanced growth at the snow line, or cumulative dust effects with gravitational instability. We will also critically review these ideas.

1. ASTROPHYSICAL CONDITIONS RELEVANT FOR PLANETESIMAL FORMATION

Dust particle, monomer particle: a solid, (sub)micrometer-sized particle present in protoplanetary disks

Planetesimal: an object ~0.1–10 km in size whose further evolution is strongly influenced by its own gravitational attraction

PPD: protoplanetary disk

The process by which (sub)micrometer-sized protoplanetary dust particles evolve to kilometer-sized planetesimals is still enigmatic. It is intimately connected with star formation, which is one of the basic processes to set the stage for planetesimal formation. As dust and gas properties change in the course of star formation, it is likely that the conditions for planetesimal formation change as well. Whether planetesimals form under certain conditions only and, thus, episodically, or throughout the entire star-formation process, is still an open question, aspects of which are the subject of this review.

Star formation happens in dense cores of molecular clouds, which collapse due to self-gravity (Bouvier et al. 2007). The collapse typically takes a few 100,000 years resulting in the formation of a central object surrounded by an accretion disk. A finite amount of the stellar mass is fed through the accretion disk onto the central object (Dullemond, Natta & Testi 2006). It is this accretion disk that provides the material for planet formation and, as such, it is most often referred to as a protoplanetary disk (PPD).

Temperatures in the inner region of these disks are initially above 2000 K, at which even the most refractory materials are in the gaseous phase (Wood 2000). Some of the material condenses into dust particles at later times or cooler locations further out in the PPD. FU Orionis outbursts, which seem to occur for solar-type stars in early stages of evolution, can lead to temperatures sufficient to evaporate dust particles in the inner 1 AU as well (Bell et al. 2000). All this is of relevance for the formation of planetesimals as it determines the properties of the primary particles, which are supposed to evolve to planetesimals and eventually to planets. An important parameter with considerable influence on the formation of planetesimals is the initial size of the dust and ice particles. Interstellar particles are thought to have sizes on the order of 100 nm (Wurm & Schnaiter 2002, Li & Greenberg 2003). The typical size of protoplanetary dust particles, however, might be slightly different owing to evaporation and recondensation in dense regions of the PPD.

Planetesimal formation is obviously an important process in the realm of solar-type stars, as we know from the Solar System that such stars can form planets. There is also ample evidence from the recent observations of extrasolar planets surrounding solar-type stars (Udry, Fischer & Queloz 2007). Nevertheless, the first planets detected outside the Solar System were orbiting pulsars, indicating that planet (and therefore planetesimal) formation is also possible around massive stars (Wolszczan & Frail 1992). It has been speculated and was recently observed in at least one case that fall-back material can form a disk surrounding the remnant star after a supernova explosion (Wang, Chakrabarty & Kaplan 2006). This lends support to the idea that planetesimal formation might not only accompany star formation but might also proceed under a variety of conditions, possibly even around dying stars.

It is also of relevance to note that the formation of a star is often not an isolated process but occurs in a star-forming region where a whole suite of stars with different masses form (Getman et al. 2006). The formation of high-mass stars then not only poses the question of planetesimal formation around these stars, but influences the environment in which low-mass stars and their surrounding circumstellar disks evolve at a much slower pace. Massive stars reach the end of their evolution in less than a million years. Their intense radiation can erode close-by PPDs (Clarke 2007), and particles ejected from a supernova explosion can enrich PPDs in, e.g., short-lived radionuclides (Wadhwa et al. 2007). These aspects must also be considered in models of the evolution of matter in the early phases of planet formation.

All this imposes a number of unknown parameters on the conditions and processes by which planetesimals might form. As seen below, at least the initial phases of planetesimal formation

might be expected to proceed in similar ways (i.e., by collisional growth) under a wide variety of conditions.

1.1. Protoplanetary Disks

Observations of spectral energy distributions and direct imaging leave no doubt that young stars are surrounded by PPDs (Dullemond et al. 2007). Typical sizes are about several hundred astronomical units (Dutrey et al. 2007). Observed lifetimes of gas-rich disks are up to about 10 million years (Wyatt, Dent & Greaves 2003; Meyer et al. 2007). So-called transitional disks seem to possess inner holes, strongly depleted in gas and micron-sized dust particles (Najita et al. 2007). It is not clear yet what triggers the formation of inner dust-free cavities. Objects like CoKu Tau 4, which are probably as young as 1 million years, can already show evidence for a large hole of 10 AU in size (D'Alessio et al. 2005). Photoevaporation by stellar radiation, stellar winds, giant planets, or photophoresis has been suggested to eventually clear the inner disk (Alexander & Armitage 2007; Takeuchi, Miyama & Lin 1996; Krauss et al. 2007), whereas photoevaporation by nearby massive stars might destroy the outer disk (Clarke 2007). Besides these extreme mechanisms, the gas density in the PPD decreases owing to viscous evolution and eventually accretion of matter onto the star.

In the standard accretion-disk scenario, turbulence is responsible for a sufficiently strong viscosity to sustain accretion with a rate of $10^{-6} - 10^{-8}\ M_{\odot}$ year^{-1} for observed and modelled PPDs and as high as $10^{-4}\ M_{\odot}$ year^{-1} during FU Orionis outbursts (Armitage, Clarke & Palla 2003; Malbet et al. 2005). This implies that matter is continuously moving toward the star, which results in a directed radial gas motion on the order of centimeters per second (Krauss et al. 2007). Any small particle coupled to the gas will move inward with the same rate and therefore on average travels a radial distance of 1 AU or more in 1 million years, somewhat depending on the distance to the star.

Turbulence is not something a priori given in PPDs. One currently discussed mechanism to sustain a sufficiently strong turbulence is the magneto-rotational instability (MRI) (Balbus & Hawley 1991). However, as a certain degree of ionization is required to sustain the MRI, which might not be available everywhere in the accretion disk, planetesimal-formation scenarios must also account for the existence of a turbulence-free zone around the midplane of the disk, a potentially important aspect with respect to particle motion and collisional planetesimal formation.

The local vertical pressure of the gas in a PPD results from hydrostatic equilibrium and can be approximated by a Gaussian decrease with height z above or below the midplane, i.e., $p = p_0 \exp[-(z/\sqrt{H})^2]$, where p_0 and H are the midplane gas pressure and the vertical scale height of the gas, respectively, which is typically 10% of radial distance to the star. Due to the uncompensated vertical component of the gravitational force of the central star and the rapid decrease of the gas pressure with height, particles settle toward the midplane. Only particles smaller than centimeters in size can efficiently be mixed up by turbulence to significant heights, whereas larger bodies gather at the midplane of the disk.

In the visible and infrared wavelength region, the process of planetesimal formation is well shielded from observation by the small dust particles that hover at the surface of the disk and render it optically thick. The existence of millimeter-sized objects in PPDs around T-Tauri stars has been inferred from observations at larger wavelengths (Wilner et al. 2005; Rodmann et al. 2006). However, observations of the formation of kilometer-sized planetesimals in PPDs are not possible. This restricts research on planetesimal formation to numerical simulations and laboratory experiments. Due to the unobservability of the planetesimal-formation process, Solar System material is also important for constraining when and how planetesimal formation is possible.

In the minimum-mass solar nebula by Hayashi, Nakazawa & Nakagawa (1985) the radial dependence of the gas density follows a power law $p \propto R^{-11/4}$. Different gas-pressure slopes, somewhat deviating from simple power laws, result from dynamic models (Papaloizou & Terquem 1999, Alibert et al. 2005). In any case, the inner regions of the accretion disks are usually much denser than their outer ranges, which is also an important factor in planetesimal formation, as collision rates of solid particles are higher in denser regions. Also of importance is the distance at which the temperature drops below the condensation temperature of water ice. Inside this snow line, only water vapor can be found, while outside water ice considerably enriches the inventory of solid particles and increases the overall mass density of solids. The snow line is located at a few astronomical units in early times of the PPD (Jang-Condell & Sasselov 2004).

Dust agglomerate, dust aggregate: an ensemble of dust particles held together by weak surface forces

1.2. Evidence from the Solar System

Grain sizes found in interplanetary dust particles attributed to comets are typically 0.3 μm in diameter (Jessberger et al. 2001), i.e., comparable to interstellar particles (Li & Greenberg 2003). However, micrometer-sized grains are also found in primitive meteorites (Scott & Krot 2005; Righter, Drake & Scott 2006). Samples from comet Wild 2, taken by the Stardust spacecraft, show a wide size range from the nanometer scale to above 10 μm (Brownlee et al. 2006; Zolensky et al. 2006), with indications that the grains ≥ 1 μm were predominantly produced in the Solar System. It is common practice in computer models of coagulation as well as in experimental studies to consider particles of about 1 μm in size as suitable analogs for dust in PPDs. This should be kept in mind as the particle size determines the sticking properties of particles (see Section 6.1). Fine-grained micrometer-sized particles stick well to each other, coarse-grained millimeter-sized sand is usually not considered very sticky. With this in mind it is curious that a large fraction of the particles found in primitive meteorites (chondrites) are millimeter-sized particles called chondrules, which can make up to 80% of a chondrite (Weisberg, McCoy & Krot 2006). Although this review is not considering the formation of chondrules, their mere existence shows that large dust aggregates must have been present in the solar nebula.

From radionuclide dating it was deduced that calcium-aluminum-rich inclusions (CAIs), which can be found in carbonaceous chondrites, are a fraction of solids that condensed fairly early after the formation of the solar nebula (Wadhwa et al. 2007). There is much evidence that a large amount of ^{26}Al was present at this time (Bizzarro, Baker & Haack 2004). Dating of iron meteorites shows that melting and differentiation of asteroids occurred in the first million years after the CAIs were formed (Wadhwa et al. 2007). If planetesimal formation was a precursor to asteroid formation it had to happen immediately after the formation of the solar nebula. On the other side, chondrites are supposed to have formed 2 to 3 million years later (Bizzarro, Baker & Haack 2004). This is consistent with ^{26}Al as a heat source, which, by the time chondrite parent bodies formed, was no longer abundant enough to lead to differentiation. If planetesimal formation occurred locally prior to asteroid formation, it proceeded over at least several million years within the early history of the solar nebula. It has been suggested that the differentiated bodies in the asteroid belt originate closer to the sun (Bottke et al. 2006). All this suggests a formation sequence starting close to the sun and migrating outward.

2. MODELS OF DISK EVOLUTION AND COAGULATION

As mentioned above, a PPD evolves over time owing to viscous evolution. Disk evolution usually refers to the gaseous component in the disk, as the gas constitutes about 99% to the disk mass. Embedded in the gaseous disk is the solid component, which initially—either caused by infall or

condensation—is in the form of microscopic dust and ice particles, well mixed with the gas and holding the remaining 1% of the disk mass. However small and well-coupled to the gas motion the dust particles are, they always possess a relative velocity to the gas, caused either by Brownian motion (for very small dust grains), by a systematic motion due to vertical settling or due to the sub-Keplerian motion of the gas, or by gas turbulence (Weidenschilling 1977). As the velocities of all these motions depend on the dust-particle mass, the dust grains also possess relative velocities, hence they can collide. It is the focus of this review to summarize our understanding of what happens in such collisions. One of the basic questions is: Do the dust particles stick together and do they form a larger aggregate after a collision? This process is termed dust agglomeration, aggregation, or coagulation. The outcome of a collision is determined by the nature and the relative velocity of the colliding particles, and the knowledge of the collision velocities and collision energies of all dust grains and aggregates is therefore of utmost importance, as detailed below. In the preplanetesimal phase, i.e., for objects smaller than ~1 km in size, the relative velocities between two particles change with increasing dust-aggregate size.

A number of coagulation models exists, which trace the size distribution of aggregates as it evolves with time in PPDs. Weidenschilling (1997, 1980) extensively modelled the formation of planetesimals and cometesimals. Dullemond & Dominik (2005) calculated the particle evolution, taking into account fractal aggregate structures and (simple) fragmentation. Ormel, Spaans & Tielens (2007) developed an algorithm to treat the porosity of the forming dust aggregates as an independent parameter. Some of these models will be more closely discussed in Section 6.3. All models result in a rapid growth of centimeter-sized dust aggregates in typically 1000 years. However, simple hit-and-stick models, which assume perfect sticking of particles in a collision, naturally do not leave many small particles behind and considerably deplete their reservoir. This would render the accretion disk optically thin after ~1000 years, which is in contradiction to the observation that small particles are abundant over millions of years in PPDs. This discrepancy can be avoided by including fragmentation as a possible outcome of a collision (Dullemond & Dominik 2005).

At their heart, all models need to incorporate a collision kernel, which describes the outcome of a collision between two dust particles or aggregates with given make up and collision velocity [see Blum (2006) for a review on dust agglomeration]. Differences in the assumptions as to how this kernel looks decide which aggregation models are able to succeed to form planetesimals and which fail and where growth gets stalled at a certain particle size. To find the correct input parameters for the kernel is a tremendous task, whose contributions from laboratory experiments are summarized in the following sections.

Agglomeration/ aggregation: process through which dust particles grow by inelastic collisions and attractive interparticle forces

3. DUST ANALOGS IN THE LABORATORY

Due to the lack of real protoplanetary dust particles, laboratory experiments require analogs with which realistic protoplanetary scenarios can be simulated. Depending on the temperature and pressure at the location of the accretion disk under consideration, various mineralogical groups, such as oxides, metals, silicates, organic materials, or ices might be of interest (Lewis 1997). Single dust-collision and -agglomeration experiments have been performed with particles from most of these groups (Nuth et al. 1994, Bridges et al. 1996, Kouchi et al. 2002), but the only systematic and partially complete parameter study has been carried out with the materials described in **Table 1**. These particles comprise medium-temperature condensates characteristic of the materials predicted to be found in PPDs around 1 AU from the solar-type central star. The α group encompasses monodisperse spherical SiO_2 (silica) particles with extremely smooth surfaces (Heim et al. 1999). These grains, although cosmochemically rather irrelevant in comparison with

Table 1 Properties of the dust particles used in the systematic dust-aggregate collision studies reviewed in Section 5

Symbol	Particle material	Density (kg m^{-3})	Particle radius (μm)	Particle shape
α_1	SiO$_2$ (amorphous)	2.0×10^3	0.95 (monodisperse)	Spherical
α_2	SiO$_2$ (amorphous)	2.0×10^3	0.50 (monodisperse)	Spherical
α_3	SiO$_2$ (amorphous)	2.0×10^3	0.76 ± 0.03 (monodisperse)	Spherical
α_4	SiO$_2$ (Aerosil 200)	2.2×10^3	0.006 ± 0.0015	Irregular
α_5	SiO$_2$	2.6×10^3	0.05–5	Irregular
β	ZrSiO$_4$	4.5–4.6×10^3	0.1−0.5	Irregular
γ	Diamond (C)	3.52×10^3	0.75 ± 0.25 (quasi-monodisperse)	Irregular
δ	MgSiO$_3$	3.2×10^3	<1.25	Irregular

the silicates (Gail 2004), have the great advantage of a direct treatability in numerical models. The difference in mineralogy between silica and the silicates has, however, a much smaller impact on the collision and sticking behavior than the size and the morphology of the single dust grains (Poppe, Blum & Henning 2000a).

Dust aggregates, i.e., the assemblages of many dust particles, can be characterized either by their anomalous mass-size relation,

$$m \propto s^D, \tag{1}$$

with m, s, and $D < 3$ being the aggregate mass, size, and the fractal dimension, or—for nonfractal dust aggregates with $D = 3$—by their volume filling factor, the fraction of space filled with dust particles,

$$\phi = \frac{\sum_i V_i}{V}, \tag{2}$$

with V_i and V being the volume of the i-th dust monomer constituting the dust aggregate and the volume of the dust aggregate, respectively. We will see in Section 5 that the volume filling factor is an essential parameter for the outcome of mutual collisions among dust aggregates.

4. ADHESION FORCES AND STICKING PROPERTIES OF MICROMETER-SIZED GRAINS

With few exceptions, protoplanetary dust aggregates are expected to be nonmagnetic (owing to the diamagnetic properties of most condensable materials in PPDs), uncharged (owing to the absence of UV photons or high-energy cosmic-ray particles deep inside the PPD), and solid (owing to the low ambient gas pressure, most liquid phases are thermodynamically unstable). Once in contact, the only attractive force between pairs of dust grains is caused by the dipole-dipole interaction between the molecules constituting the two dust particles. If static electrical dipoles are present (e.g., in the case of water-ice particles), the attractive force is stronger than in the case of induced dipoles (van der Waals attraction). However, the Hamaker constant describing the intrinsic strength of the attractive dipolar force is only weakly material dependent (Israelachvili 1992).

Two spherical particles in contact always exert an attractive force onto one another. As a result of the attraction, the particles flatten elastically and form a circular contact area. Due to this enlarged contact surface, the attractive force increases. The pull-off force, necessary to separate two spherical particles in contact, was calculated by Johnson, Kendall & Roberts (1971) to be

$$F_{JKR} = 3\pi\eta R, \qquad (3)$$

with η and R being the surface energy of the particle material and the reduced radius, respectively. The reduced radius is given by $R = r_1 r_2/(r_1 + r_2)$, with r_1 and r_2 being the radii of the two particles in contact. Taking into account noncontact forces in the vicinity of the contact area, Derjaguin, Muller & Toporov (1975) derived

$$F_{DMT} = 4\pi\eta R \qquad (4)$$

for the pull-off force. Heim et al. (1999) experimentally confirmed the linear relation between the pull-off force and the reduced radius. They measured a surface energy for spherical SiO_2 particles of radii between 0.5 μm and 2.5 μm (the α_1–α_3 particles in **Table 1**) of $\eta = 0.019$ J m^{-2} when using Equation 3 and $\eta = 0.014$ J m^{-2} when using Equation 4. It is interesting to note that the pull-off force is independent of the elastic properties of the particle material.

Although larger dust particles have higher (static) sticking forces, according to Equations 3 and 4, (dynamic) collisions among smaller dust particles more likely lead to sticking than collisions between large grains. This was experimentally demonstrated by Poppe, Blum & Henning (2000a) for spherical SiO_2 grains impinging into smooth solid surfaces. Although SiO_2 particles with radii of 0.24 μm stuck at velocities below $\sim$1.9 m s^{-1}, larger grains with radii of 0.53 μm possessed a sticking threshold velocity of $\sim$1.2 m s^{-1}.

However, Poppe, Blum & Henning (2000a) found a much stronger influence of the grain morphology on the sticking behavior. Whereas micrometer-sized spherical particles possess a rather well-defined threshold velocity around $\sim$1 m s^{-1}, below which they always and above which they never stick, irregular-shaped dust particles show a considerable sticking probability even for impact velocities as high as several tens of meters per second in collisions with rigid walls (Poppe, Blum & Henning 2000a).

5. EXPERIMENTS ON DUST-AGGREGATE COLLISION AND GROWTH

In this section, we concentrate on dust agglomeration and dust-agglomerate collision experiments relevant for 1 AU. These experiments cover a wide range of aggregate sizes and collision velocities for (mostly) silicate particles and therefore offer a rather complete picture of the physical processes relevant for dust agglomeration in PPDs around solar-type stars at 1 AU. A few experiments dealt with the collision properties of volatile particle materials, such as organics and ices. As we are far from having the full picture of the collision and agglomeration behavior of these particles, we only briefly mention these experimental findings in Section 7.1.

To systemize the physical description of the experiments reviewed here, we have ordered the dust-agglomeration and aggregate-collision experiments into three groups:

- **Group A**: Experiments in which the colliding dust agglomerates have approximately identical mass. The numerals following the letter A increase with increasing mass and (for conditions within PPDs) collision velocity of the collision partners.
- **Group B**: Experiments in which individual microscopic solid dust particles (monomer grains) collide with a macroscopic dust agglomerate. The numerals following the letter B increase with increasing collision velocity.
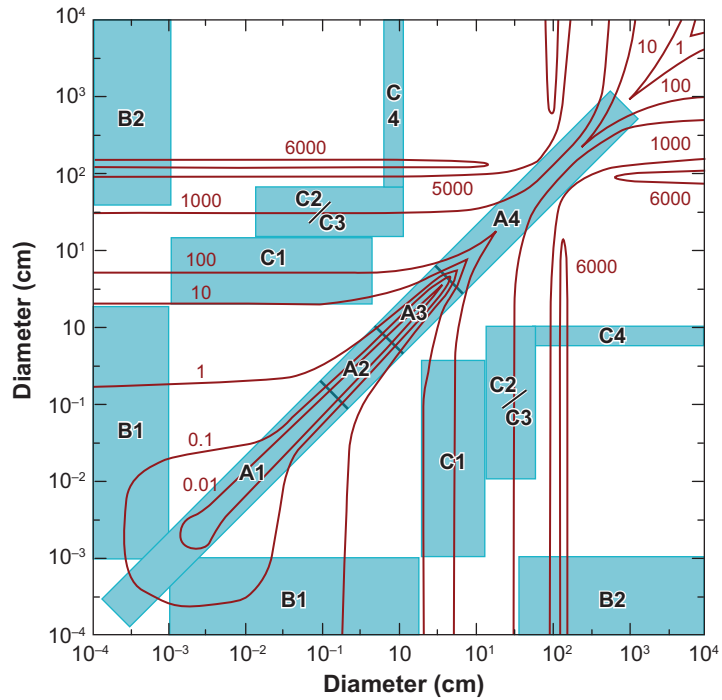
Figure 1

The parameter space of the experiments described in Section 5. The blue boxes indicate the applicability of the individual experiments to the collision scenario described by Weidenschilling & Cuzzi (1993) for a minimum-mass solar nebula. In the background, the original contour plot of the collision velocities (in cm s^{-1}) for all pair-collisions by Weidenschilling & Cuzzi (1993) is shown. The data from Weidenschilling & Cuzzi (1993) are valid for 1 AU and for a turbulent gas velocity of $\sim$10 m s^{-1}.

- **Group C**: Experiments in which a dust-agglomerate projectile impacts a larger dust-agglomerate target. The numerals following the letter C increase with increasing collision velocity.

Figure 1 shows the parameter space of the experiments to be described in this section. The boxes indicate the applicability of the individual experiments to the collision scenario described by Weidenschilling & Cuzzi (1993). In the background, the original contour plot for all pair-collisions from Weidenschilling & Cuzzi (1993) is shown. The data from Weidenschilling & Cuzzi (1993) are valid for 1 AU and for a turbulent gas velocity of $\sim$10 m s^{-1}.

5.1. Experiments A1: Fractal Aggregate Growth

Name: Fractal aggregate growth
References: Blum et al. 1998, 2000, 2002; Wurm & Blum 1998; Krause & Blum 2004
Dust sample: α_1, α_2, γ (see **Table 1**)
Projectile: Fractal dust agglomerates
Target: Same as projectile
Collision velocities: 10^{-4}–0.26 m s^{-1}
Miscellaneous: Laboratory experiments, microgravity experiments onboard the space shuttle and a sounding rocket
Application to PPDs: Earliest stage of agglomeration

Fractal dust agglomerate: dust agglomerates for which a mass-size relation $m \propto s^D$ with $D < 3$ exists

When the dust grains are still very small, their coupling to the ambient gas is so strong that the resulting drift motions are extremely slow. Hence, differential settling is not the main driver for mutual collisions among the grains (Weidenschilling 1977). Brownian motion of the micrometer-sized particles, although very inefficient for the global transport of the grains, dominates the collision rate. As Brownian motion relies on the equipartition of energy among all constituents of a thermodynamic system (Einstein 1905), the solid particles possess an average thermal velocity relative to the gas at rest of

$$v_t = \sqrt{\frac{3kT}{m}},$$ (5)

where k, T, and m denote the Boltzmann constant, the temperature of the gas, and the mass of the dust grains. As the gas is very tenuous, the coupling between gas and dust-particle motion happens on the frictional timescale given by

$$\tau_f = \varepsilon_\tau \frac{m}{\sigma_g} \frac{1}{\rho_g \bar{v}},$$ (6)

where σ_g, ρ_g, $\bar{v}$, and ε_τ are the geometric cross section of the dust particle or aggregate, the gas density, the mean molecular speed, and a correction factor. Blum et al. (1996) found experimentally $\varepsilon_\tau = (0.68 \pm 0.10)$, whereas Meakin, Donn & Mulholland (1989) theoretically derived $\varepsilon_\tau = 0.58$. The corresponding length scale $l = v_t \tau_f$ usually exceeds the size of the dust particles or aggregates considered in the Brownian-motion growth phase so that all collisions among the dust aggregates can be treated as ballistic. This places a strong constraint to all realistic experimental approaches. Paszun & Dominik (2006) have shown with computer simulations that the morphology of the growing dust aggregates depends on the above length scale.

Blum et al. (1998, 2002, 2000) and Krause & Blum (2004) describe experiments in which the Brownian-motion driven agglomeration of micrometer-sized dust particles was observed. Due to the fact that in the laboratory (in which the particles are subjected to a constant acceleration g) the sedimentation velocity of a dust aggregate $v_s = g\tau_f$ always exceeds the thermal velocity v_t, the experiments were performed under long-duration microgravity conditions. A dispersion of almost perfectly deagglomerated dust grains into a rarefied gas was produced, and the temporal evolution of the forming agglomerates was observed by long-distance microscopy. The above studies found that the sticking probability in the collisions was unity and that the forming dust agglomerates possessed a fractal structure with a fractal dimension of $D \approx 1.4$ (see inset of **Figure 2**), coinciding with the predictions of Paszun & Dominik (2006) for the gas pressure in the experiments of $p \approx 100$ Pa. Extrapolating to the even lower gas pressures in PPDs, we expect the dust aggregates to have fractal dimensions of $D \approx 1.5$. This is lower than predicted by Kempf, Pfalzner & Henning (1999), owing to the previous negligence of Brownian rotation (Blum et al. 2006b), which seems to play some role in this early protoplanetary aggregation stage (Paszun & Dominik 2006).

The above-mentioned experiments also showed that the mean mass of the forming aggregates grows as a power-law in time, $\bar{m} \propto t^{1.7}$ (**Figure 2**). The mass distribution of the fractal aggregates around the mean mass is quasi-monodisperse (i.e., very narrow) and can be modelled using Smoluchowski's rate equation (Smoluchowski 1916, Blum 2006).

Due to the fact that the Brownian-motion induced collision velocity decreases with increasing aggregate mass (see Equation 5), the importance of this growth phase in PPDs is limited to aggregate sizes not exceeding a few tens of micrometers. Beyond this stage, differential drift motions of the fractal dust aggregates dominate. Differential settling is the most important source for collisions of submillimeter dust aggregates. Blum et al. (1998) experimentally simulated this in the laboratory with the help of gravity by injecting a cloud of dust grains into a rotating chamber filled with a rarefied gas. The rotational motion of the gas and the friction between gas and dust
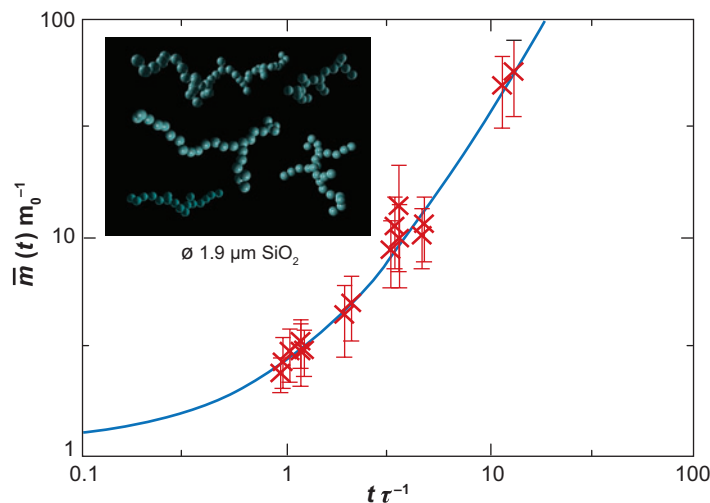
Figure 2

The temporal evolution of the mean aggregate mass (in units of the monomer-grain mass) in the fractal growth scenario (see Section 5.1) with Brownian motion as the source for aggregate-aggregate collisions [taken from Krause & Blum (2004)]. The data points are taken from the experiments by Krause & Blum (2004), while the solid curve is the solution (Equation 13) to a monodisperse Smoluchowski equation. On the abscissa, the time is normalized to the collisional timescale for monomer grains. The inset shows examples of fractal dust aggregates found in the space shuttle experiments by Blum et al. (2000).

forced the dust particles to circle about a stable horizontal axis off-center from the rotational motion of the experiment chamber. With this setup, experiment durations of several minutes were possible in which the dust particles did not hit the chamber walls. Similar to the results of the Brownian-motion experiments, Blum et al. (1998) also found, for differential settling as the source for collisions, that the forming dust aggregates were fractal in structure, with a fractal dimension of $D = 1.7$, and possessed a quasi-monodisperse mass distribution. Wurm & Blum (1998) investigated the sticking probability for fractal aggregates and found that all collisions in the velocity range of millimeters-to-centimeters per second lead to sticking.

Wurm & Blum (1998) also investigated the evolution of a cloud of dust particles with random relative velocities up to a few tens of centimeters per second. As in the previously described experiments, fractal aggregate growth ($D = 1.9$) with quasi-monodisperse mass spectra was found. Hit-and-stick collisions in an ensemble of dust grains lead to fractal aggregates with fractal dimensions $D < 2$. Self-consistently, such low fractal dimensions require hit-and-stick collisions between similar-sized aggregates, i.e., almost monodisperse mass distributions, as demonstrated in **Figure 3**.

5.2. Experiments A2: Fractal-Aggregate Sticking and Compaction
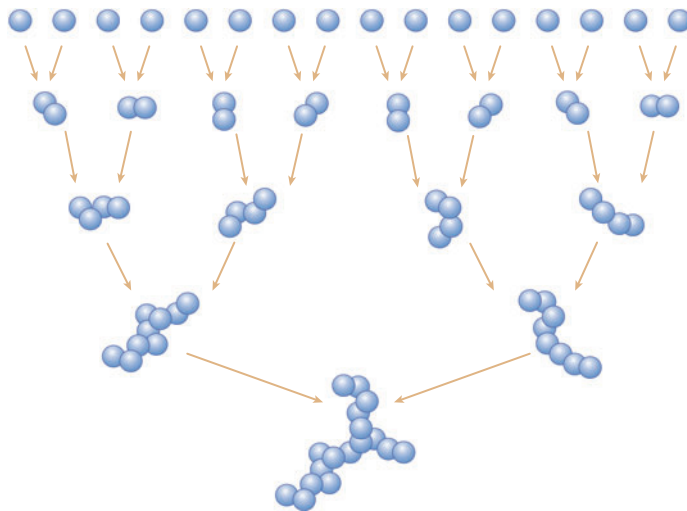
Name: Fractal-aggregate sticking and compaction
References: Dominik & Tielens 1997, Blum & Wurm 2000, Wada et al. 2007
Dust sample: α_1, α_2, δ (see **Table 1**)
Projectile: Fractal dust agglomerates
Target: Solid steel foil, solid Si_3N_4 (for largest impact velocities), compacted dust aggregate (for intermediate impact velocities), loose dust aggregate (for lowest impact velocities)
Collision velocities: 0–30 m s^{-1}

Miscellaneous: Laboratory experiments, microgravity experiments in drop tower, numerical studies

Application to PPDs: Sedimentation phase

The experiments A1 have shown that low-energy hit-and-stick collisions lead to fractal dust aggregates (see **Figures 2** and **3**). However, the situation in PPDs is such that the collision velocities between fractal dust aggregates are only slowly increasing with aggregate mass, owing to a rather unaffected surface-to-mass ratio of dust aggregates with $D < 2$. Whereas the collision velocities are rather constant, the collision energy increases with increasing aggregate mass. Hit-and-stick collisions require a strong resistance of the grains against rolling or sliding in off-center collisions. Applied to collisions between fractal dust aggregates, Dominik & Tielens (1997) developed a molecular-dynamics code and predicted a threshold energy of

$$E_{im} = 5 E_{roll}, \tag{7}$$

above which collisions of (small) fractal dust aggregates lead to compaction (**Figure 4**). Wada et al. (2007) used a similar approach and found for much larger fractal aggregates that compaction already starts at

$$0.1 E_{roll} \leq E_{im} \leq 1 E_{roll}. \tag{8}$$

Here, E_{im} and E_{roll} are the collision energy of the fractal dust aggregates and the rolling-friction energy of the monomer grains. The latter is the energy dissipated when two spherical dust grains roll over a quarter of their circumference (Dominik & Tielens 1997). Maximum compaction of the colliding dust aggregates is achieved when the impact energy is

$$E_{im} = n_k E_{roll}; \tag{9}$$

n_k is the number of contacts in the aggregates (Dominik & Tielens 1997, Wada et al. 2007). For fractal aggregates, the number of contacts in an aggregate equals the number of monomers, owing to the quasi-monodisperse growth nature of those aggregates (see **Figure 3**). Although the sticking probability in such collisions is still unity, the forming dust aggregates are compacted and lose their fractal morphologies. Blum & Wurm (2000) performed microgravity impact experiments with fractal ($D \sim 1.9$) dust aggregates and observed—in agreement with the predictions by Dominik & Tielens (1997) and Wada et al. (2007)—a hit-and-stick behavior for very low impact velocities.
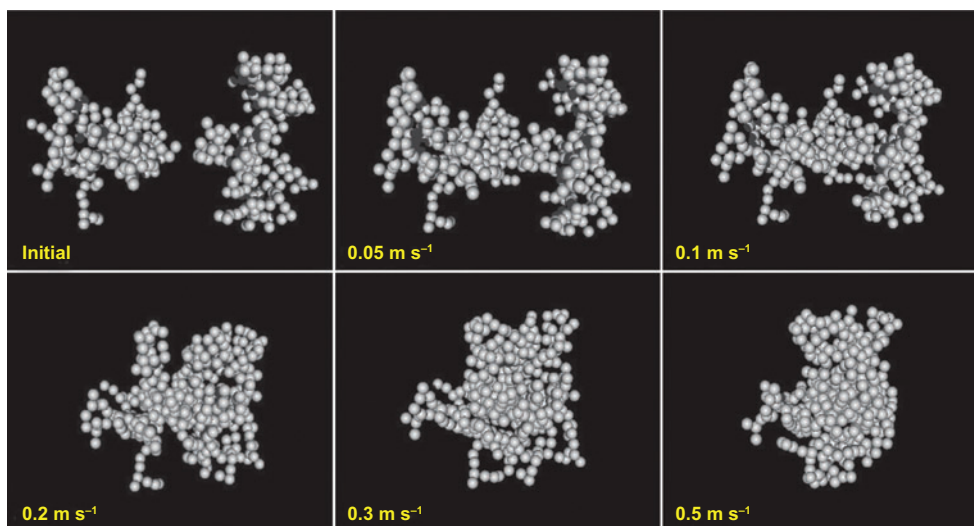
Figure 4

Compaction of fractal dust aggregates in mutual collisions (see Section 5.2). Molecular-dynamics simulations by D. Paszun & C. Dominik, University of Amsterdam. The upper left panel shows the initial dust aggregates before the collision. The subsequent panels show the results of the collisions with increasing velocity. The effect of restructuring and compaction is clearly visible.

Increasing the impact speed, the aggregates were compacted, but still stuck to the dusty target. However, above a threshold velocity of ~ 1 m s^{-1}, the impinging dust aggregates fragmented so that no further growth took place. Based on the measurements of the interparticle force in grain-grain contact and grain-grain rolling by Heim et al. (1999), Blum & Wurm (2000) showed that their experimental results quantitatively agree with the theoretical predictions. Heim et al. (1999) found rolling-friction energies of the order of 10^{-15} J for spherical micrometer-sized SiO$_2$ monomers. Thus, the experimental results—although achieved with impacts of single fractal aggregates into much larger dusty and solid targets—can also be applied to collisions between similar-sized dust aggregates.

5.3. Experiments A3: Aggregate Bouncing

Name: Bouncing collisions of nonfractal dust agglomerates
References: Blum & Münch 1993, D. Heißelmann, H. Fraser & J. Blum (unpublished data)
Dust sample: β, α_4, α_3 (see **Table 1**)
Projectile: Nonfractal, millimeter-sized, quasi-spherical, and irregular-shaped aggregates with $\phi = 0.26$ (β), $\phi = 0.03$ (α_4), $\phi = 0.15$ (α_3)
**Target:** Same as projectile
Collision velocities: 0.15–3.9 m s^{-1}
Miscellaneous: Microgravity experiments in the laboratory and in parabolic flights
Application to PPDs: Sedimentation and drift phase

Nonfractal dust agglomerate: dust agglomerates for which a mass-size relation $m \propto s^3$ exists; nonfractal dust agglomerates may still be extremely porous

The experiments and numerical simulations presented in the previous section show that collisions among dust aggregates in PPDs will eventually lead to nonfractal (but potentially still highly porous) dusty objects. Although A2 collisions between fractal dust aggregates can be energetic enough to cause compaction, sticking probabilities are still high. This changes drastically if the colliding dust aggregates are nonfractal, as experiments by Blum & Münch (1993) and
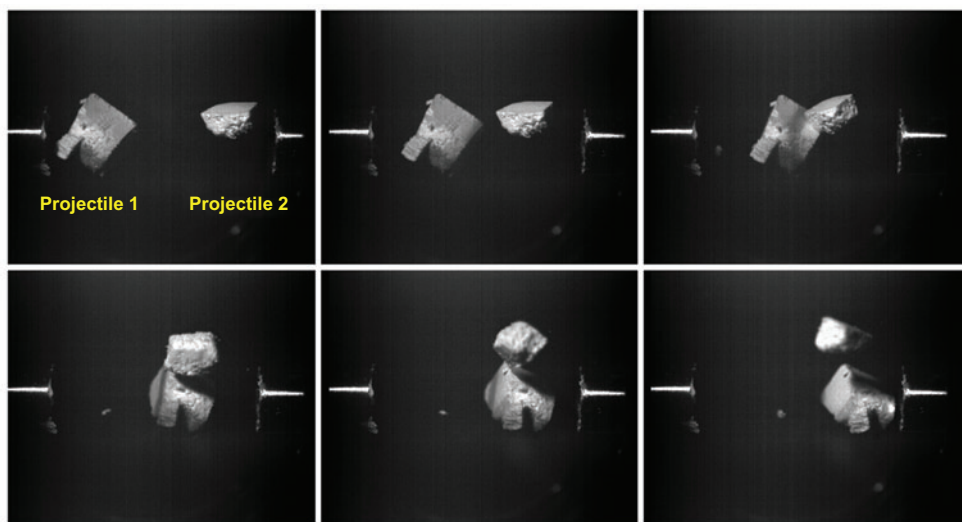
Figure 5

Bouncing of two irregular-shaped, nonfractal, but highly porous dust aggregates ($\phi = 0.15$) at a relative velocity of ~ 0.4 m s^{-1} (see Section 5.3). The images were taken with a high-speed camera in a microgravity experiment onboard a parabolic-flight aircraft. The field of view is 24×20 mm^2. Figure by D. Heißelmann, H. Fraser & J. Blum (unpublished data).

D. Heißelmann, H. Fraser & J. Blum (unpublished data) show. Both experimental investigations studied collisions among millimeter-sized dust aggregates under vacuum and weightlessness conditions, Blum & Münch (1993) in the laboratory and D. Heißelmann, H. Fraser & J. Blum (unpublished data) onboard a parabolic aircraft. The collision velocities were in the range of 0.15–3.9 m s^{-1}. Regardless of the packing density of the dust agglomerates, i.e., whether the colliding dust aggregates were highly porous (D. Heißelmann, H. Fraser & J. Blum, unpublished data) or rather compacted (Blum & Münch 1993), collisions between pairs of millimeter-sized nonfractal dust aggregates never led to sticking (**Figure 5**). The reason for the altered sticking behavior of macroscopic nonfractal dust aggregates lies in the fact that the contact area between two equal-sized spherical bodies is rather small (compared to the case in which a spherical dust aggregate impacts a flat dusty target; see Section 5.7). Following the closest approach in a collision, the two spherical bodies start to separate. The above-mentioned experiments have shown that for central collisions the typical kinetic energy after a collision is $\sim 5\%$ of the kinetic energy before the first contact. Thus, the adhesion forces across the contact area must be sufficiently strong to result in the sticking of the two dust aggregates in the rebound phase of the collision. However, the small contact area and the measured low tensile strengths of the dust aggregates of $\sim 10^2$–10^4 Pa (Blum et al. 2006a) prevent similar-sized dust aggregates above a size of ~ 1 mm from sticking in the collision.

From these experiments, we learn that the previous growth channel for protoplanetary dust, in which (almost) equal-sized aggregates collide and stick, is no longer available under protoplanetary conditions. Although the experiments by Blum & Münch (1993) and D. Heißelmann, H. Fraser & J. Blum (unpublished data) gave no indication for mass transfer between or compaction of the dust aggregates in single collisions, the aggregates can be considerably altered by a multitude of impacts. C. Güttler & J. Blum (unpublished data), who observed the evolution of initially cubic-shaped high-porosity dust aggregates on a 50-μm metal mesh and a solid glass plate due to multiple bouncing with velocities of $\lesssim 1$ ms^{-1}, used X-ray tomography to study the internal compaction of the bodies. They found that after ~ 1000 collisions, the millimeter-sized dust aggregates had a

roundish shape and had developed a densified rim of 0.3-mm thickness with a peak density a factor of two to three higher than the original material. As experiments by Blum & Schräpler (2004) and Blum et al. (2006a) showed, such a compaction causes a considerable change in the mechanical behavior of the dusty material (see Sections 5.5 and 5.7).

SPH: smooth particle hydrodynamics

5.4. Experiments A4: Aggregate Fragmentation

Name: Fragmentation in collisions between equal-sized nonfractal dust agglomerates
References: Blum & Münch 1993; Wurm, Paraskov & Krauss 2005b; Schäfer, Speith & Kley 2007; C. Güttler & J. Blum, unpublished data
Dust sample: β, α_3, α_5 (see **Table 1**); ice (numerical simulations)
Projectile: Nonfractal, submillimeter- to centimeter-sized, quasi-spherical dust agglomerates with $\phi = 0.26$ (β), $\varphi = 0.36$ (α_3), $0.34 \leq \phi \leq 0.36$ (α_5); 1-m-sized ice agglomerates (numerical simulations)
Target: Same as projectile (β, ice), solid SiO_2 (α_3), compacted α_5 ($\phi = 0.34$)
Collision velocities: 1.0–25 m s^{-1}
Miscellaneous: Laboratory and microgravity laboratory experiments, numerical simulations
Application to PPDs: Sedimentation and drift phase, turbulence-induced collision velocities

If the collision energy of the dust aggregates is further increased, experiments have shown that fragmentation takes the role of the dominating process. Collisions between equal-sized dust aggregates can either be studied directly with arbitrary impact parameter (Blum & Münch 1993) or simulated by the impact of one dust aggregate into a solid target (central collisions) (C. Güttler & J. Blum, unpublished data; Wurm, Paraskov & Krauss 2005b). A major difference between these two methods is that pair collisions can be studied in free fall so that gravity has no influence on the outcome, whereas impacts into solid targets may suffer from gravitational influence. However, for the faster collisions, the importance of gravity has been shown to be negligible (Wurm, Paraskov & Krauss 2005b).

Blum & Münch (1993) investigated collisions between pairs of millimeter-sized dust aggregates consisting of micrometer-sized ZrSiO$_4$ (sample β in **Table 1**) dust grains in free fall. They found that collisions above ~1 m s^{-1} lead to the break-up of the aggregates. The mass loss from the original projectiles increases with increasing impact velocity and decreases with increasing impact angle, i.e., for noncentral collisions. For the highest collision velocity of ~3.8 m s^{-1} investigated by Blum & Münch (1993), the mass distribution of the fragments follows a power-law. Recent experiments by C. Güttler & J. Blum (unpublished data), who investigated the impact of dust aggregates consisting of micrometer-sized SiO$_2$ spheres (sample α_3 in **Table 1**) onto solid glass targets, fully confirm these findings. Wurm, Paraskov & Krauss (2005b) investigated the impacts of several millimeter-sized dust aggregates consisting of polydisperse SiO$_2$ grains (sample α_5 in **Table 1**) into compressed targets of the same material at velocities of ~7–25 m s^{-1}. Whereas in the former experiments at rather low impact velocities the largest fragment still possessed a considerable mass fraction of the original projectile, the higher impact velocities (and the slightly larger projectiles) investigated by Wurm, Paraskov & Krauss (2005b) led to a fragment mass distribution, which peaks at an aggregate size of 550 μm. It should be noted that Wurm, Paraskov & Krauss (2005b) observed growth at the same time as detailed in Section 5.9.

Schäfer, Speith & Kley (2007) studied the collision between equal-sized ice aggregates using a smooth particle hydrodynamics (SPH) code (**Figure 6**). They deduced from their simulations that fragmentation is an important outcome in collisions of higher velocity, particularly for aggregates with low compressive and tensile strengths (see Section 5.5). Low values of compressive and tensile

strength result in the production of many more fragments as if the aggregates were harder and stickier. Thus, the knowledge of the mechanical strengths of protoplanetary dust aggregates is of utmost importance for the modelling of the collisional outcome.

5.5. Experiments B1: Nonfractal Aggregate Growth

Name: Growth of nonfractal, high-porosity dust agglomerates by ballistic particle-cluster collisions

References: Blum & Schräpler 2004, Blum et al. 2006a

Dust sample: α_3, α_5, γ (see **Table 1**)

Projectile: Single grains

Target: Dust agglomerate with 2.5-cm diameter, $\phi = 0.15$ (α_3), $\phi = 0.11$ (γ), $\phi = 0.07$ (α_5)

Collision velocities: $\sim$0.1–1 m s^{-1}

**Miscellaneous:** Laboratory experiments

Application to PPDs: Sedimentation and drift phase; agglomeration in the presence of a source of small grains (condensation, fragmentation)

The experiments A1–A4 have shown that the growth of protoplanetary dust agglomerates cannot proceed arbitrarily long through sticking collisions of equal-sized dust aggregates. Due to impact compaction and the small interaction cross section between similar-sized dust aggregates, the maximum aggregate size that can be achieved under protoplanetary-disk conditions at 1 AU along this avenue is $\sim$1 mm (Blum 2004). For the further direct growth of preplanetesimal bodies, only collisions between aggregates of very different sizes are potential candidates. Although the previous growth process leads to quasi-monodisperse mass distributions, there still might be plenty of small dust particle and aggregates present, owing to radial and vertical mixing, condensation processes, or fragmentation of larger aggregates.

Blum and colleagues (Blum & Schräpler 2004, Blum et al. 2006a) studied the extreme case of a large high-porosity dust aggregate being fed by micrometer-sized dust grains at impact velocities

Figure 7

A random ballistic deposition aggregate grown in the laboratory as an example of a high-porosity dust aggregate formed by the addition of monomer grains in hit-and-stick collisions (see Section 5.5). The image shows a dust aggregate with a 2.5-cm diameter and a volume filling factor of $\phi = 0.11$, consisting of ~1.5-µm diamond particles (sample γ in **Table 1**).
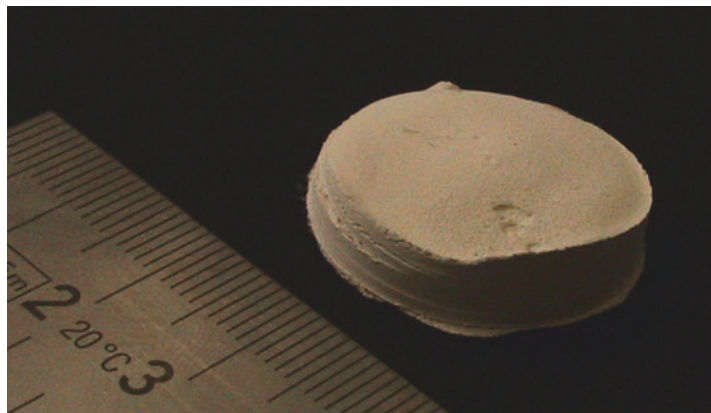
below the restructuring limit (see Section 5.2). In free space, such a scenario leads to nonfractal bodies described as ballistic particle-cluster aggregates (BPCA) (Vold 1959, 1963; Sutherland 1966). A similar aggregate morphology with identical porosity to the BPCA can be achieved by random ballistic deposition (RBD) (Watson et al. 1997, Blum & Schräpler 2004). RBD is much easier to realize in the laboratory by unidirectional flow of small dust grains onto a fixed target. Blum & Schräpler (2004) showed that the laboratory-grown RBD aggregates have a volume filling factor of $\phi = 0.15$ if monodisperse spherical dust grains are used, identical to the numerical predictions by Watson et al. (1997). Thus, hit-and-stick collisions below the restructuring threshold (see Dominik & Tielens 1997) will lead to high-porosity dust agglomerates. Blum et al. (2006a) also showed that deviations from the monodispersity and sphericity of the projectile grains lead to even fluffier RBD aggregates (**Figure 7**). In addition to sample α_3, they also used samples α_5 and γ (see **Table 1**). Deviation from sphericity (sample γ) resulted in a reduction of the volume filling factor to $\phi = 0.11$, whereas a wide size distribution of irregular-shaped monomers (sample α_5) yielded an even lower volume filling factor of $\phi = 0.07$.

Deviations from the hit-and-stick behavior and thus the growth of more compact dust aggregates are expected when the impact energy of the impinging monomer grain exceeds the limit for rolling-friction (Dominik & Tielens 1997, Wada et al. 2007) (see Equations 7 and 8 in Section 5.2). For a spherical dust grain of 1-µm diameter, the rolling-friction energy can be extrapolated from Heim et al. (1999) to $E_{roll} = 5 \times 10^{-16}$ J. As the mass of a 1-µm SiO_2 grain is $m = 1.4 \times 10^{-15}$ kg, the threshold velocity for RBD aggregates is $v_{RBD} = (0.2 \dots 10 E_{roll}/m)^{1/2} = 0.3 \dots 1.9$ ms^{-1}.

For the determination of the outcome of collisions among high-porosity dust aggregates, Blum et al. (2006a) measured the compression behavior and the tensile strengths of their laboratory RBD specimens. They found that the compressive strength of their centimeter-sized dust aggregates increased from $200 \leq C \leq 500$ Pa for the most porous samples ($0.07 \leq \phi \leq 0.15$) to 10^5 Pa $\leq C \leq 5 \times 10^5$ Pa for highly compacted aggregates ($0.20 \leq \phi \leq 0.33$). The range of compressions chosen by Blum et al. (2006a) simulates impacts with velocities between 1 m s^{-1} and 50 m s^{-1}, i.e., the range of velocities relevant for the preplanetesimal stage. The tensile strength did not vary that much and ranged from $200 \leq T \leq 1000$ Pa for $0.07 \leq \phi \leq 0.15$ to $T = 6300$ Pa for extremely highly compressed samples with $\phi = 0.66$.

5.6. Experiments B2: Aggregate Erosion

RBD: random ballistic deposition

Name: Erosion of nonfractal, high-porosity dust agglomerates by ballistic particle-cluster collisions

References: R. Schräpler & J. Blum, unpublished data)

Dust sample: α_3 (see **Table 1**)

Projectile: Single grains

Target: Dust agglomerate with a 1-cm diameter, consisting of α_3 grains, $\phi = 0.15$, $\phi \approx 0.6$ (compacted)

Collision velocities: 15–60 m s^{-1}

Miscellaneous: Laboratory experiments

Application to PPDs: Large dust agglomerates ($\gtrsim$30 m) in the presence of a source of small grains (turbulent mixing, condensation, fragmentation)

Whereas the experiments described in Section 5.5 were performed at impact velocities <1 m s^{-1} to avoid restructuring, R. Schräpler & J. Blum (unpublished data) concentrated on high-velocity impacts of single dust grains into macroscopic dust aggregates. At impact velocities between 15 m s^{-1} and 60 m s^{-1}, this simulates the conditions in the solar nebula, when bodies $\gtrsim$30 cm in diameter encounter small dust grains (see **Figure 1**). When using very porous dust aggregates as targets, R. Schräpler & J. Blum (unpublished data) found that after an initial phase, in which an individual impacting dust particle eroded up to 10 particles from the target agglomerate, the impacting particles passivated the agglomerates against erosion by compacting their surface layers. Owing to this effect, the initial erosion was stopped within the experimental uncertainties for velocities up to 30 m s^{-1}. For higher velocities, the erosion was reduced by an order of magnitude. For the environment of PPDs this means that large bodies can in principle survive the continuous bombardment by the ever-ambient small grains, if they get compacted by impacts or otherwise passivated, e.g., through sintering. Paraskov, Wurm & Krauss (2006) showed that the direct erosional influence of the surrounding gas onto a large dusty body, whose relative velocity with respect to the gas is several tens of meters per second, is small. However, it is still unclear what fate bouncing or eroded dust particles have in a gas flow, as they initially possess rather low velocities to the parent body (see Section 7.2). Future work must concentrate on this.

5.7. Experiments C1: Nonfractal-Aggregate Sticking and Compaction

Name: Collisions between different-sized high-porosity dust agglomerates

References: Langkowski, Teiser & Blum 2008; J. Teiser & J. Blum, unpublished data

Dust sample: α_3, α_5, γ (see **Table 1**)

Projectile: Dust agglomerate 0.2–3 mm in diameter, $\phi = 0.15$ (α_3), $\phi = 0.11$ (γ), $\phi = 0.07$ (α_5); solid SiO$_2$ spheres with 1.1-mm diameter

Target: Dust agglomerate with 2.5-cm diameter, $\phi = 0.15$ (α_3), $\phi = 0.11$ (γ), $\phi = 0.07$ (α_5); arbitrary impact angle; target surface flat or curved

Collision velocities: $\sim$0.1–3 m s^{-1}

Miscellaneous: Microgravity experiments in drop tower

Application to PPDs: Whenever broad size range of dust agglomerates is present; experimental results valid for projectile sizes $\sim$10 μm–$\sim$5 mm and target sizes $\sim$2 cm–$\sim$10 cm

The investigations described in the previous sections concentrated on the two extreme scenarios of collisions among equal-sized aggregates as well as between large aggregates and microscopic monomer grains. The experiments to be described in the following sections consequentially deal with impacts between different-sized but macroscopic dust aggregates. As Weidenschilling & Cuzzi (1993) have shown (see **Figure 1**), the impact velocities of small dust agglomerates do not drastically differ from those of the monomer grains. It is therefore not of primary importance to

study extremely low impact velocities, as we know that they will inevitably lead to sticking. It is
more interesting to investigate what happens if a dust aggregate of a given size hits a much larger
aggregate at an arbitrary impact angle. Experimentally, it is sufficient if the larger aggregate's size
exceeds that of the impinging dust aggregate by a factor ~10, as the region influenced by the
collision will not be very much larger than the projectile size at the moderate-velocity conditions
relevant for planetesimal formation.

Langkowski, Teiser & Blum (2008) studied the impacts of millimeter-sized high-porosity
projectiles into cylindrical RBD (see Section 5.5) dust aggregates of 2.5-cm diameter and ~1-cm
height (see **Figure 7** for an example). The projectile and target dust aggregates consisted of α_3,
α_5, and γ particles with volume filling factors of $\phi = 0.15$, $\phi = 0.11$, and $\phi = 0.07$, respectively.
Impact velocities ranged from ~0.1 m s^{-1} to ~3 m s^{-1}, and impact angles were almost randomly
distributed. J. Teiser & J. Blum (unpublished data) performed similar impact experiments with
millimeter-sized solid glass beads into large dust aggregates consisting of α_3 particles ($\phi = 0.15$).
Both experiments consistently find the surprising fact that there is a threshold velocity above
which the impinging projectiles stick. This threshold velocity slightly increases with increasing
obliquity of the impact, i.e., normal impacts more likely result in sticking than grazing incidences
(**Figure 8**). However, projectiles with sufficiently low impact velocity or mass also stick to the
target. The qualitative difference between the two types of sticking is that while very low im-
pact energy results in adhesion of the projectile to the surface of the target agglomerate, sticking at
the higher velocities is entirely caused by a geometrical effect, i.e., the projectiles penetrate the
(soft) target so deeply that they cannot escape. J. Blum (unpublished data) successfully modelled
this bifurcated sticking behavior by using Langkowski, Teiser & Blum's (2008) findings that the
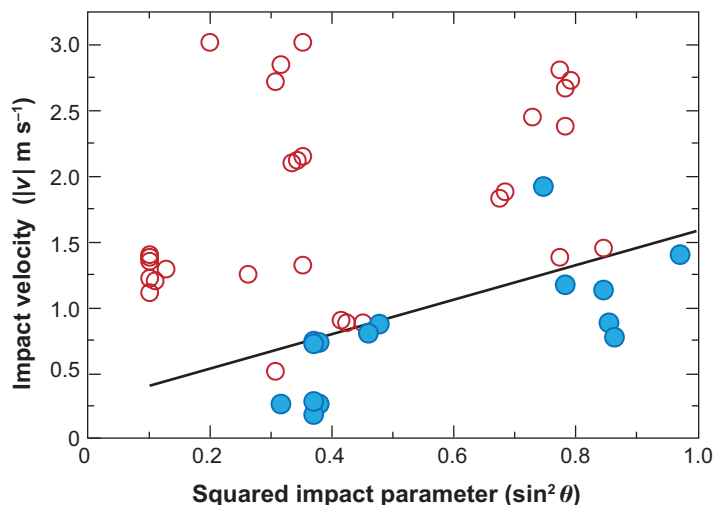
Figure 8

Bouncing (*filled circles*) and sticking (*open circles*) in impacts of millimeter-sized solid glass spheres with
high-porosity ($\phi = 0.15$) centimeter-sized dust aggregates, consisting of α_3 particles (see Section 5.7). The
solid line is an estimate of the threshold velocity between sticking and bouncing, which increases with
increasing obliquity angle θ of the impact, denoted by the squared impact parameter $\sin^2(\theta)$ (J. Teiser
& J. Blum, unpublished data).

crater volume excavated by nonsticking impacts can be described by

$$V_{cr} \propto E_{im,\,n}^{\nu}, \tag{10}$$

with $E_{im,\,n}$ being the normal component of the projectile's impact energy. Langkowski, Teiser & Blum (2008) determined the exponent in Equation 10 to $\nu = 0.75$. In the model by J. Blum (unpublished data) the projectiles are destined to stick if they penetrate into the target deeper than one projectile radius. For lower impact velocities, the balance between rebound energy, determined by the coefficient of restitution, and tensile energy, given by the product of the tensile force and the breaking length, is relevant for the condition of sticking. Measurements of tensile force and breaking length can be found in Blum & Schräpler (2004). Measurements of the coefficient of restitution, i.e., the ratio between rebound and impact velocity of bouncing dust-aggregate projectiles, were performed by Langkowski, Teiser & Blum (2008); they find a wide range of values between close to 0 and ~0.6, with typical values around 0.1–0.3. The model by J. Blum (unpublished data) predicts that the velocity range in which projectiles bounce (because they are both too slow to deeply penetrate into the target and too fast for the effective dissipation of their restitution energy by tensile forces) increases with increasing projectile size. For projectiles smaller than ~1 mm, all collisions should result in sticking. This still needs to be experimentally confirmed.

As the experiments by Langkowski, Teiser & Blum (2008) show, all collisions above ~1 m s^{-1} impact velocity lead to the compaction of the target (and supposedly also of the projectile) agglomerate in the vicinity of the impact location. Hence, a sequence of collisions will lead to the compaction of the entire ensemble of colliding bodies. As we have seen in Section 5.5, compression of dust aggregates leads to the increase of the compressive strength and, thus, to a decrease in the ability to absorb energy in a collision. Hence, we can expect that compacted dust aggregates collide more elastically than very fluffy dusty bodies. To evaluate the strength of this effect, Langkowski, Teiser & Blum (2008) estimated the dynamic impact pressure and found that the onset of compaction happens at 100 Pa $\leq p_{dyn} \leq 1000$ Pa, closely matching the static pressure at which Blum et al. (2006a) found compaction (see Section 5.5). For the estimation of the highest impact pressure that a body in the preplanetesimal phase may encounter, we can approximate the dynamic pressure by

$$p_{dyn} = \frac{1}{2}\rho v^2, \tag{11}$$

with ρ and v being the mass density of the colliding bodies and the collision velocity, respectively. For the highest protoplanetary collision velocity of $v \approx 50$ m s^{-1}, and for the (initial) mass density of the aggregates, $\rho = 300$ kg m^{-3}, we get $p_{dyn} = 3.75 \times 10^5$ Pa, for which Blum et al. (2006a) found high compressions of $\phi \approx 0.3$ (see Section 5.5). Thus, any protoplanetary body that goes through collisions at 50 m s^{-1} velocity should be rather compacted. This will clearly influence the sticking behavior in subsequent collisions, as the experiments described in Section 5.9 show.

Sirono (2004) theoretically investigated a similar scenario using an SPH code. He found that two dust aggregates stick upon a collision if the compressive strength is smaller than the tensile strength and if the impact velocity does not exceed 4% of the sound speed. However, the experiments by Langkowski, Teiser & Blum (2008) demonstrate that sticking also occurs for aggregates, whose tensile and compressive strengths are comparable. Measurements of the sound speed of RBD aggregates consisting of α_3 particles yielded values of 30 m s^{-1}. Thus, Sirono (2004) predicts sticking for all velocities below 1.2 m s^{-1}, while above this value cratering or fragmentation should dominate. However, Langkowski, Teiser & Blum (2008) find that even for impact velocities of ~3 m s^{-1} (their highest experimental values) sticking of the two colliding aggregates occurs (see **Figure 8** for comparison, but mind that the projectiles in this case were solid glass beads).

5.8. Experiments C2: High-Velocity Cratering and Fragmentation

Name: Impact cratering

References: Wurm, Paraskov & Krauss 2005a; Paraskov, Wurm & Krauss 2007

Dust sample: α_5 (see **Table 1**)

Projectile: Dust agglomerate $\sim$5–10 mm in diameter, $\phi = 0.34$ (compressed); solid spheres 5–8 mm in diameter

Target: 6-cm diameter, consisting of sifted α_5 dust with typical granule sizes of 0.1–0.5 mm in diameter [$0.12 \leq \phi \leq 0.26$; porosity has two components: (*a*) microporosity of the individual granules ($0.4 \lesssim \phi_1 \lesssim 0.5$), (*b*) macroporosity due to the packing of the granules ($\phi_2 \approx 0.4 \lesssim \phi_2 \lesssim 0.5$); $\phi = \phi_1 \times \phi_2$); compacted targets consisting of α_5 dust ($\phi = 0.34$)

Collision velocities: 3.5–37.5 m s^{-1}

Miscellaneous: Laboratory and microgravity experiments in drop tower; impact direction normal to target surface (central collisions)

Application to PPDs: Experiments are relevant for impacts of centimeter-sized projectiles into larger dusty objects of $\sim$0.3–0.8-m diameter

Wurm, Paraskov & Krauss (2005a) investigated impacts of centimeter-sized compressed-dust projectiles into dust targets of 6-cm diameter under vacuum conditions. The targets were prepared by sifting α_5 dust into a target tray. The mesh size in most experiments was 0.5 mm, while in some experiments mesh sizes of 0.09 and 0.025 mm were used. Thus, the target consisted of a rather dense packing of dust granules of $\leq$0.5 mm ($\leq$0.09 mm, $\leq$0.025 mm) diameter. The granules themselves consisted of densely packed α_5 particles, so that the targets showed both micro- and macroporosity. The projectiles were accelerated by a spring-loaded device, which provided impact velocities of 16.5–37.5 m s^{-1}. Wurm, Paraskov & Krauss (2005a) observed that, owing to the loose structure of the porous target, a crater of 2–3 cm in diameter and a few millimeters in depth formed (**Figure 9**). The observations showed that the crater originates from the impact-compaction of the target material and still encompasses most of the mass of projectile and target, as only few ejecta were detected originating at the crater. However, considerable mass loss from the target of $\gg$10 times the projectile mass was deduced. Ejection velocities of the surface granules were quite uniform over the whole target surface with typical velocities of 0.10–0.15 m s^{-1}. Thus, for such impacts under solar-nebula conditions, an extended surface range of at least a few times the projectile diameter can be affected by a high-velocity impact. Due to the low surface gravity of meter-sized objects, any such released fragments would inevitably be lost from the surface under vacuum conditions. However, Wurm, Paraskov & Krauss (2005a) argue that the gas flow toward/through larger bodies in PPDs can drive slow ejecta back to the target (Wurm, Blum & Colwell 2001a, 2001b) (see Section 7.2). If this occurs, the experiments by Wurm, Paraskov & Krauss (2005a) indicate that net mass growth is possible in high-speed conditions even for large bodies.

Figure 9

Image of an impact crater stemming from a high-velocity impact of compact dust aggregates into a porous dust target (see Section 5.8).
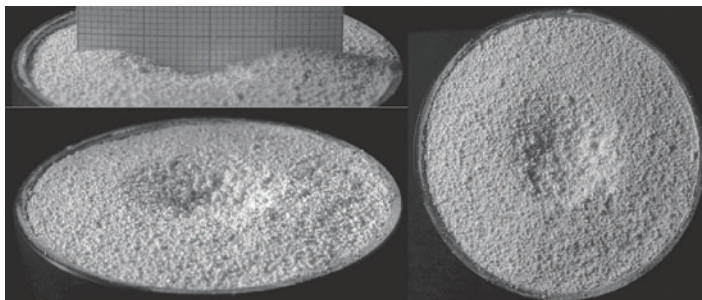
Paraskov, Wurm & Krauss (2007) augmented the above-described experiments with investigations of similar impacts under microgravity conditions in the velocity range of 3.5–21.5 m s^{-1}. Qualitatively, they confirmed the results by Wurm, Paraskov & Krauss (2005a). In addition, they found that for loose targets, the majority of the ejecta stems from the entire free target surface (and not from the projectile); in addition the ejection velocities of these fragments were in the range 0.03–0.12 m s^{-1} and were preferentially ejected normal to the target surface. Ejecta were also observed at the opposite side of the target. Paraskov, Wurm & Krauss (2007) conclude that, owing to the preparation technique, the target had both properties of a granular medium and a still significant cohesion, and that dilatancy (granular medium) and cohesion (dust) were responsible for the observed effects.

5.9. Experiments C3: Mass Accretion in High-Velocity Impacts of Compact Aggregates

Name: High velocity collisions with mass accretion
References: Wurm, Paraskov & Krauss 2005b; Paraskov, Wurm & Krauss 2007
Dust sample: α_5 (see **Table 1**)
Projectile: Compacted dust agglomerate ($\phi = 0.34$), diameter 5–10 mm
Target: Compacted dust agglomerate ($\phi = 0.34$), diameter 5 cm
Collision velocities: 6–25 m s^{-1}
Miscellaneous: Impact direction normal to target surface (central collisions); laboratory experiments; drop tower experiments
**Application to PPDs:** Projectile several millimeters to centimeters in size, impacting a target of up to several decimeters in size

The previous experiments unambiguously showed that the collisional outcome changes from sticking to bouncing and fragmentation once the collision velocities exceed ∼1 m s^{-1} for equal-sized collision partners. In the fragmentation regime, the higher the impact velocity, the more destructive the collisions are. However, the experiments by Wurm, Paraskov & Krauss (2005b) showed the unexpected result that even at impact velocities above 10 m s^{-1} partial sticking of a dusty projectile to a target body is possible if the target consists of compacted dust or is otherwise passivated (see also Section 5.6). Wurm, Paraskov & Krauss (2005b) observed impacts of compact dust-aggregate projectiles 5–10 mm in size into 5-cm compact dusty targets at velocities of 6–25 m s^{-1} under vacuum conditions. Three main conclusions can be drawn from these experiments: (*a*) Most important for planetesimal growth, the experiments show that even at an impact velocity of 25 m s^{-1}, a target can gain mass in a collision. **Figure 10** shows the accretion efficiency as a function of collision velocity. (*b*) A threshold for accretion occurs at about 13 m s^{-1} for the given experiment parameters. Somehow counterintuitively, accretion occurs at the higher collision velocities, not at the slow collisions. This can be interpreted as a transition from mostly elastic (slow) collisions to inelastic (fast) collisions. In the latter cases, enough kinetic energy is dissipated by the fragmentation process to allow part of the projectile to stick to the target. (*c*) Smaller dust aggregates are produced and ejected during the projectile break-up. Whenever accretion occurs, the accretion efficiency is 50%, accounting for half of the projectile mass. The remaining 50% of the projectile mass is redispersed to small dust particles. Therefore, growth and fragmentation occur concurrently in the same collision event.

The target is not a completely passive wall in these collisions, e.g., slower projectiles can leave imprints in the target after rebound. A small amount of material ejected might also stem from the target. Other details still need to be worked out. It was verified under microgravity by Paraskov, Wurm & Krauss (2007) that gravity has no influence on the outcome of the collisions and that the

Accretion efficiency (the difference in target mass before and after an impact with respect to the projectile mass) in high-velocity impacts of compact dust aggregates into compact dust targets (see Section 5.9). Figure taken from Wurm, Paraskov & Krauss (2005b).
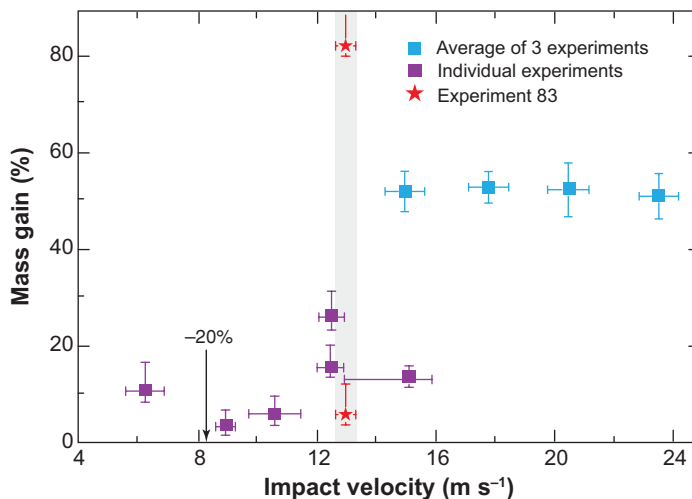
impact does not influence the backside of a 5-cm thick compact target. Ongoing experiments with multiple impacts have so far shown that the irregular surface structure caused by partial sticking of previously impacted projectiles does not prevent further mass gain in subsequent collisions (J. Teiser, personal communication).

5.10. Experiments C4: High-Velocity Cratering and Fragmentation

Name: High velocity growth limit

References: J. Teiser & G. Wurm, unpublished data

Dust sample: α_5 (see **Table 1**)

**Projectile:** Compacted dust agglomerate ($\phi = 0.34$), diameter 5–10 mm

Target: Compacted dust agglomerate ($\phi = 0.34$), diameter 12 cm

Collision velocities: 25–50 m s^{-1}

Miscellaneous: Impact direction normal to target surface (central collisions); laboratory experiments

Application to PPDs: Projectile size of 1 cm; target size from several decimeters to planetesimal size

The experiments summarized in Section 5.9 were limited to an impact velocity of 25 m s^{-1} and impact energies below 0.1 J. A partial growth was possible under the conditions detailed in Section 5.9. In current experiments, J. Teiser & G. Wurm (unpublished data) find that at slightly higher impact energies, net erosion of the target occurs even when the target consists of compacted dust aggregates. The projectiles create an impact crater of several millimeters in depth with two distinct sections. A depression of 1-cm diameter forms in the center corresponding to the projectile size. Somewhat shallower, surrounding this central crater, is a region of ~1-cm extension, in which dust is chipped off during the impact (**Figure 11**). This is probably due to elastic waves spreading from the impact site. However, as this is work in progress, further analysis is required before more definite statements can be made on this subject. We speculate that net growth in collisions at maximum collision velocities (~50 m s^{-1}) might be possible with millimeter-sized dust projectiles for which the impact energy remains below about 0.1 J but that erosion occurs for larger (and smaller) projectiles.
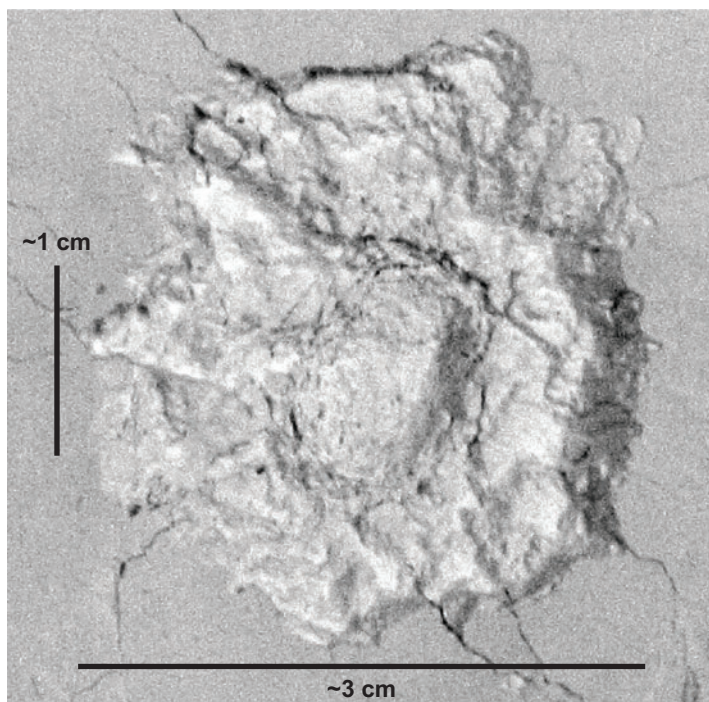
6. SYNTHESIS AND CONCLUSIONS

The results from the systematic dust-aggregate collision experiments described in the previous section are summarized in **Figure 12** in a pictorial diagram, similar to **Figure 1**. Shown on both axes are the sizes of the colliding dust aggregates. Boxes in blue refer to collisions, which unambiguously result in sticking for the velocities calculated by Weidenschilling & Cuzzi (1993) (see **Figure 1**). Yellow denotes bouncing, and orange indicates mass loss by erosion, cratering, or fragmentation. From **Figure 12** it is clearly visible that direct growth is—under the conditions of PPDs—possible for dust-aggregate sizes below ~10 cm. For bodies exceeding ~1 m in size, experiments and numerical simulations predict mass loss as the dominating process. The results summarized in **Figure 12** are valid for micrometer-sized dust particles consisting of refractory materials.

6.1. The Collisional Outcome as a Function of Monomer-Grain Size

Unfortunately, there is no systematic investigation about the influence of the monomer-grain size on the collision behavior of dust aggregates, i.e., how **Figure 12** changes if particles much smaller or much larger than 1 μm in size dominate. However, a few publications dealing with dust-aggregate collisions have used monomer grains ranging from nanometers to submillimeters in size.

In a series of impact experiments under microgravity conditions, Colwell and coworkers demonstrated that impacts of centimeter-sized solid projectiles into dust beds consisting of typically 75–250 μm-sized grains lead to the ejection of fragments even if the impact velocities are as low as ~0.25 m s^{-1} (Colwell & Taylor 1999, Colwell 2003, Colwell et al. 2008). As we have seen in Sections 5.8–5.10, impact velocities of several m s^{-1} are required to reach the same results for dust aggregates consisting of micrometer-sized particles. Sticking of the centimeter-sized solid projectiles to the regolith-type dust targets was observed for impact velocities ≲0.2 m s^{-1} (Colwell 2003).
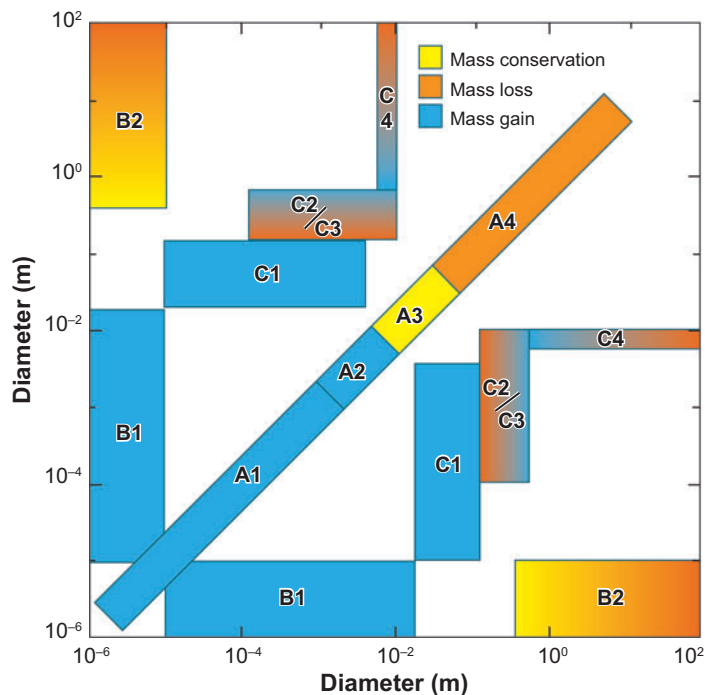
Figure 12

Overview of the results of the laboratory experiments described in Section 5. The blue, yellow, and orange boxes denote sticking, bouncing, and fragmentation for collisions between two protoplanetary dust aggregates of the sizes indicated at the axes of the diagram, respectively. Collision velocities were implicitly taken from Weidenschilling & Cuzzi (1993) (see **Figure 1**) for a minimum-mass solar nebula. It is clearly visible that direct growth of protoplanetary bodies ≳10 cm is not possible.

Experiments by Blum & Wurm (2000) have shown that fractal dust aggregates consisting of micrometer-sized monomer grains possess a rather sharp threshold velocity above which sticking no longer occurs (see Section 5.2). For $s = 0.5$ μm SiO_2 spheres, $s = 0.95$ μm SiO_2 spheres, and $s < 1.25$ μm irregular $MgSiO_3$ particles, Blum & Wurm (2000) found threshold velocities of 3.5 m s^{-1}, 1.2 m s^{-1}, and 2.2 m s^{-1}, respectively.

Experiments by Reißaus et al. (2006) showed that single 2.5 nm $\leq s \leq$ 25 nm Al_2O_3 particles and fractal aggregates thereof stick to a solid carbon target at an impact velocity of 400–500 m s^{-1}. Particles and aggregates consisting of graphite 5 nm $\leq s \leq$ 10 nm in size stick to the target for impact velocities as high as 1000–1100 m s^{-1}.

From these three experimental investigations we can draw the conclusion that the size of the monomer grains in aggregate collisions has a decisive influence on the collision and sticking behavior. This is graphically shown in **Figure 13**, where we plotted the velocity below which sticking occurs for the impact experiments by Reißaus et al. (2006) and Colwell (2003) for nanometer-sized and 100-μm-sized dust particles, respectively, along with the results shown in Section 5.2 for micrometer-sized grains. For the most likely protoplanetary grain sizes of 0.1 μm $\lesssim s \lesssim$ 10 μm, we can approximate the threshold velocity for sticking by

$$\frac{v_{\text{th}}}{1 \text{ m s}^{-1}} = \left(\frac{s}{1 \text{ μm}}\right)^{-x},\tag{12}$$

with $x \approx 1$. Much smaller grain sizes result in $x > 1$, whereas much larger grain sizes yield $x < 1$.
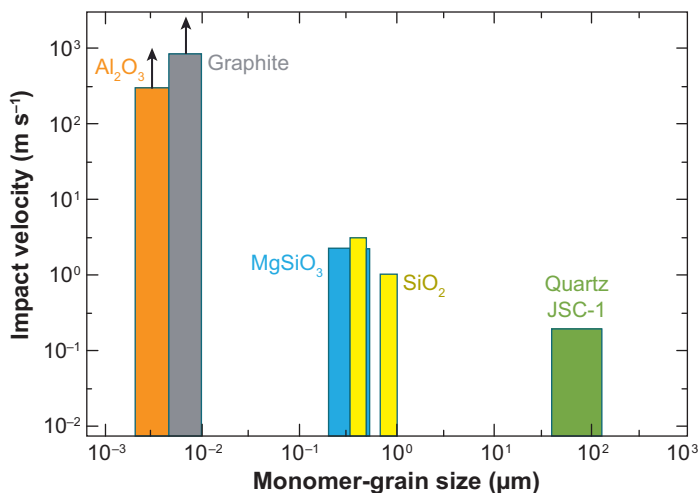
Figure 13

The sticking range for dust aggregates as a function of the dust-monomer size. The data in the nanometer-, micrometer-, and 100 μm-size range are taken from Reißaus et al. (2006), Blum & Wurm (2000), and Colwell (2003), respectively. Note that Reißaus et al. (2006) measured impacts (and sticking) at one velocity only so that their data for the nanometer-sized grains must be considered as lower limits. Whereas the experiments by Reißaus et al. (2006) and Blum & Wurm (2000) were performed with (fractal) dust-aggregate projectiles impacting solid targets, Colwell (2003) measured impacts of solid projectiles into nonfractal dust-aggregate targets.

6.2. The Onset of Aggregate Growth is Always Fractal

The experiments described in Section 5.1 leave no doubt that the onset of protoplanetary dust growth must proceed via fractal aggregation, independent of the monomer-grain size. As long as the impact energies of the colliding dust aggregates are below the restructuring threshold described by Equation 7, any collision will result in a hit-and-stick-type freezing of the two aggregate structures. This behavior inevitably leads to fractal structures of the aggregates with $D < 2$ and consequentially to a quasi-monodisperse aggregate-mass spectrum (see **Figure 3**). Depending on the mean collision velocity of the dust aggregates, the mean aggregate mass will either grow with a power-law or exponentially with time (Blum 2006). If the mean collision velocity of dust aggregates with mass m scales as $v \propto m^\alpha$ and the collision cross section of two equal-sized fractal aggregates scales as $\sigma \propto m$ (Blum 2006), we get as an approximation for the temporal evolution of the mean aggregate mass

$$m(t) = \left[-\alpha \left(\frac{t}{\tau_c} + c \right) \right]^{-\frac{1}{\alpha}} \tag{13}$$

for $\alpha \neq 0$ and

$$m(t) = \exp \left(\frac{t}{\tau_c} + c \right) \tag{14}$$

for $\alpha = 0$, respectively (Blum 2006). The constant c is determined by the initial conditions of the growth process considered. The collision timescale τ_c is given by

$$\tau_c = \frac{1}{\mu_0 \sigma_0 v_0}, \tag{15}$$

with μ_0, σ_0, and v_0 being the number density, collision cross section and collision velocity of the monomer grains, respectively. More detailed numerical work has confirmed the general power-law, quasi-monodisperse growth (Weidenschilling & Cuzzi 1993; Dullemond & Dominik 2005; Ormel, Spaans & Tielens 2007).

6.3. How Far Does the Growth of Dust Aggregates Proceed at 1 AU?

Although a detailed modelling of the agglomeration process at 1 AU, taking into account the experimental results from the previous sections, is still missing, we can conclude that we expect a rather sharp transition from sticking to nonsticking (either in the form of bouncing or as fragmentation) whenever the mean collision velocity exceeds the threshold value v_{th}, which is a strong function of the characteristic size (radius) of the monomer grains constituting the colliding dust aggregates (see Equation 12 in Section 6.1 and **Figure 13**).

It is not a simple endeavor to unambiguously predict the monomer size of the dust grains in PPDs. Astronomical observations are usually most sensitive to grain sizes comparable to the wavelength, while meteoritic investigations often suffer from parent-body alterations. Taking together evidence from astronomy, meteorite research, in-situ and remote-sensing observations from cometary nuclei, and sampling of interplanetary dust particles of likely cometary origin, it seems clear that the monomer-grain size should fall between a few tenths of a micrometer and a few micrometers. Thus, the threshold velocity for direct collisional sticking is $v_{th} \lesssim 3$ m s^{-1}, which means that dust agglomeration at best proceeds to decimeter sizes in a direct, pair-collisional manner (see **Figure 1**). Due to the rather high collision energies of centimeter- to decimeter-sized protoplanetary dust aggregates, the largest bodies are likely to be subjected to impact compaction. Static experiments by Blum & Schräpler (2004) and Blum et al. (2006a) suggest volume filling factors of $\phi \approx 0.1$; however, first X-ray-tomography observations following impact experiments have shown considerably higher local compactions of up to $\phi \approx 0.3$ (M. Krause, J. Teiser & J. Blum, unpublished data).

Blum (2004) developed a simplified model of the evolution of protoplanetary dust aggregates at 1 AU in the solar nebula. Taking into account that (*a*) only collisions with velocities lower than the threshold $v_{th} \approx 1$ m s^{-1} lead to sticking, (*b*) the collision velocities are governed by Brownian motion and sedimentation and are not statistically distributed (i.e., there are no lucky winners), (*c*) the transition from the Brownian motion to the sedimentation-dominated region is sharp, (*d*) the initial growth is fractal (see Sections 5.1 and 6.2), followed by a nonfractal growth stage (see Section 5.2), and (*e*) the growth process in the fractal regime is purely monodisperse (see **Figure 3**) and in the nonfractal regime bi-disperse, Blum (2004) found a rapid growth from the initial micrometer-sized dust grains to decimeter-sized nonfractal dust aggregates within $\sim 10^3$ years with no further growth when the threshold velocity for sticking was reached.

In a much more sophisticated model, Dullemond & Dominik (2005) basically confirmed these results with their models S5 and S6 for fractal and nonfractal dust aggregates. Their model S4, which assumes compact particles and a sticking probability of unity for all aggregate sizes and which takes into account all relevant collision sources (Brownian motion, differential settling, turbulence), results in the formation of planetesimals but seems unrealistic when compared to the experimental results shown in Section 5 (see **Figure 12**). However, by introducing (perfect) fragmentation for collisions above a threshold (their model SD1), Dullemond & Dominik (2005) found that bodies larger than 1 m in size can form. Due to the statistical nature of individual collisions, these lucky winners never underwent a fragmentation event. In that case, the mass distribution function is essentially flat between monomer and centimeter-aggregate sizes with a dip at decimeter-sized bodies and a local maximum at larger aggregates.

Ormel, Spaans & Tielens (2007) developed a dust-agglomeration model for PPDs, which treats the porosity of the growing dust aggregates as an independent parameter. High-porosity dust aggregates have an increased collisional cross section and sediment much slower toward the midplane of the disk, owing to the increased surface-to-mass ratio. This effect keeps much larger dust aggregates aloft before they rain out from regions above or below the midplane. The model by Ormel, Spaans & Tielens (2007) predicts the growth of centimeter- to decimeter-sized porous dust aggregates within a few thousand years, before the simulations were stopped owing to the rain-out of the dust aggregates. In a recent paper, Brauer, Dullemond & Henning (2008) found that dust growth stops even at ∼1 cm in size or below, owing to fragmentation.

7. HOW TO MAKE PLANETESIMALS?

Due to the experimental findings discussed in the previous sections, it seems unlikely to form planetesimals by direct collisional sticking (see **Figure 12**). Once the dust aggregates have reached sizes of a few centimeters, the average collision velocity increases above the threshold level for direct sticking (see Equation 12). For the formation of gravitationally active planetesimals, other mechanisms have to be found. A variety of recipes for the growth of planetesimals have been proposed, which are briefly reviewed in this section. We start with ideas about very sticky materials (Section 7.1) not obeying Equation 12, then discuss methods for secondary agglomeration (Section 7.3), which can reduce individual collision velocities below the sticking threshold. Thereafter we review a model of the dust enhancement at the snow line that can lead to much lower mean collision velocities (Section 7.3), before we refer to recent ideas about cumulative effects and gravitational instability in an ensemble of dust aggregates (Section 7.4).

However done, the formation of kilometer-sized planetesimals has to happen fast, as large bodies possess a rather short lifetime owing to their effective inward drift motion (Weidenschilling 1977). A maximal drift velocity of $\sim 10^2$ m s^{-1} is reached for meter-sized bodies in typical PPD models. Such a drift velocity results in a lifetime of ∼100 years. Thus, any model explaining the growth over this meter-size barrier has to be extremely fast to prevent the radial drift of the macroscopic bodies.

7.1. Special Material Conditions

Equation 12 predicts the threshold velocity, below which sticking of dust aggregates occurs (see Section 6.1). However, deviations from Equation 12 are possible for particle materials with enhanced interaction forces, e.g., organic matter, ice, magnetic materials, or electrically charged grains.

7.1.1. Sticky organic materials. Kouchi et al. (2002) performed impact experiments using mixtures of organic materials representative for the organic matter in PPDs. Due to the viscoelastic behavior of organic matter in a narrow temperature regime, the sticking threshold velocity can be considerably increased. Kouchi et al. (2002) found that a 1-cm copper sphere, dropped onto a copper block coated with a 1-mm thick layer of organic material, stuck for impact velocities as high as 5 m s^{-1} at a temperature of ∼250 K. For lower and higher temperatures, the sticking threshold velocity decreased. The tensile strength, a measure of the sticking force between the copper sphere and the organic layer, was as high as 10^5 Pa, and was therefore increased by one to two orders of magnitude over the tensile strengths of refractory dust aggregates (see Section 5.5).

7.1.2. Frost. Besides organic materials, frost of water and other ices has been proposed to foster the stickiness of protoplanetary dust grains. Hatzes et al. (1991) performed collision experiments with single solid ice spheres of 5-cm diameter and inferred that the presence of an uncompressed frost layer 10–100 μm thick causes sticking in collisions with less than 3×10^{-4} m s^{-1}. Bridges et al. (1996) measured the cohesion force between macroscopic H_2O- and CO_2-frost-coated ice particles and deduced for the conditions in PPDs that collisions with less than 4×10^{-3} m s^{-1} velocity lead to sticking between decimeter-sized ice particles. The physical mechanism responsible for the sticking is interlocking of the surface structures of the two colliding bodies. Although frost obviously improves the stickiness of protoplanetary dust, large objects should nonetheless possess collision velocities of several tens of meters per second, so potential frost layers seem an implausible explanation for further growth.

7.1.3. Magnetic particles. The kinetics of dust growth via agglomeration is governed by the collision frequency of the dust agglomerates, which, in turn, is a linear function of the collision cross section and the relative velocity of the colliding dust aggregates (see Blum 2006 for details). Growth rates can potentially be considerably increased if long-range forces act on the dust aggregates. In that case, the geometric collision cross section is no longer relevant but must be substituted by some enhanced interaction area. Long-range forces can originate in magnetic, electric, or gravitational interaction.

Nuth et al. (1994) and Nuth & Wilkinson (1995) described laboratory experiments and theoretical background of aggregation experiments with ~20 nm-sized magnetized iron grains. Very rapid agglomeration along with the formation of spiderweb or net structures was found and explained by a considerable enhancement of the collision cross section owing to long-range magnetic interaction. Nübold & Glassmeier (2000) argued that even macroscopic protoplanetary bodies might be magnetized if their growth was augmented by magnetic forces, thus opening an avenue for future in situ analysis of, e.g., cometary nuclei. Dominik & Nübold (2002) showed that in the initial, Brownian motion-dominated protoplanetary growth phase, dust aggregation proceeds much faster if the dust grains are magnetized. Nübold et al. (2003) experimentally confirmed this and showed that the forming dust aggregates have fractal structures with a fractal dimension of $1.2 \leq D \leq 1.5$. However, the extensive work by Nuth et al. (1994), Nuth & Wilkinson (1995), Nübold & Glassmeier (2000), Dominik & Nübold (2002), and Nübold et al. (2003) shows that magnetic enhancement of protoplanetary dust aggregation probably only contributes at the very earliest stages of dust growth, owing to a strong decrease of the magnetically enhanced collision cross section with increasing relative velocity. So far, it has not yet been shown that, under the conditions prevailing in PPDs, meter-sized or larger objects can form via magnetic forces.

7.1.4. Electric runaway growth. Runaway growth is a process by which the mass of a single dust aggregate increases much faster than the masses of all other particles in the system (see Blum 2006 for details). Theoretically, this is possible whenever the exponent in the mass dependence of the collision kernel $K(m) = \beta(m)\sigma(m)v(m)$ is stronger than linear, i.e., if $K(m) \propto m^{\xi}$, with $\xi > 1$. Here, $\beta(m)$, $\sigma(m)$, and $v(m)$ are the sticking probability, the collision cross section, and the collision velocity between two dust aggregates with masses m, respectively. For nonfractal and uncharged dust aggregates, the collision cross section scales as $\sigma(m) \propto m^{2/3}$. For drift- or turbulence-induced relative velocities, the scaling is $v(m) \propto m^{1/3}$, and the sticking probability does not increase with increasing dust-aggregate mass. Hence, $\xi \leq 1$ throughout the PPD.

This situation can change if the dust aggregates are charged. Ivlev, Morfill & Konopka (2002) have shown that runaway growth can occur in an overall neutral system of (positively and negatively) charged dust particles. It is important to know that the dominating process leading to an

overgrowth of the collision cross section is the charge-dipole interaction, which is always attractive. In that case, the condition for runaway growth changes to $K(m, Q) \propto m^\xi Q^\zeta$, with $\xi + \zeta/2 > 1$. Here, Q is the average charge on a dust aggregate. If we assume a constant sticking probability in collisions between dust aggregates, the condition for runaway growth can be fulfilled for $\zeta > 0$. F. Mokler & G.E. Morfill (unpublished data) show that this seems to be possible for PPDs, particularly at the snow line. Under favorable conditions, dust aggregates with masses of 1 kg or more might form by charge-dipole–induced dust gelation.

7.2. Secondary Agglomeration

Although the average collision velocity of large protoplanetary dust aggregates is higher than the limit for bouncing or fragmentation (yellow and orange regions in **Figure 12**), collisions might still result in a mass gain of the larger body, if secondary effects, like the influence of the ambient gas flow and impact charging, are taken into account.

7.2.1. Aerodynamic reaccretion. We have discussed above that collisions between dust aggregates with sizes $\gtrsim$10 cm do not lead to direct sticking. However, as Wurm, Blum & Colwell (2001a,b) point out, when dust aggregates of very different sizes collide at velocities that lead to cratering or fragmentation, the escaping fragments can be carried back to the larger body. This is possible because the larger object moves at a much higher velocity with respect to the gas. Thus, the emerging fragments quickly couple to the gas flow and can become recaptured by the larger body. If the gas flow around the larger aggregate is of Knudsen type, i.e., if the mean free path of the gas molecules exceeds the size of the dust aggregate, Wurm, Blum & Colwell (2001a,b) show that the captured fragments have secondary collision velocities below the sticking threshold. Sekiya & Takeda (2003) show that this aerodynamic reaccretion can potentially lead to the growth of bodies as large as about ten times the mean free path of the gas molecules. Thus, the meter-sized barrier can be overcome in the outer reaches of protoplanetary accretion disks only. Wurm, Paraskov & Krauss (2004) argue that the growth can proceed even further than the limit given by Sekiya & Takeda (2003) if the growing body is partially gas-permeable. In this case, gas streamlines penetrate the larger dust aggregate so that secondary collisions of fragments with the surface of the large aggregate are still feasible. Sekiya & Takeda (2005) counter that this effect is, however, quantitatively unimportant for meter-sized bodies if the pores within are small.

The efficiency of the aerodynamic reaccretion (for submeter-sized bodies) is strongly dependent on the properties of the ejecta in the preceding collision. The product of the coupling time of the ejecta to the gas motion—a direct measure of the ejecta size—and the ejecta velocity give the stopping distance with respect to the gas. Too-fast escape trajectories will not lead to the reaccretion of the ejecta. The ejecta escape angle from the surface is also important to derive conditions for a secondary collision. Thus, it is important to determine ejecta sizes, velocities, and escape angles. The experimental work by Wurm, Paraskov & Krauss (2005a,b) showed that high-speed collisions can lead to two different ejection mechanisms of small dust particles (see Sections 5.8 and 5.9) with very different ejection angles and velocities. Impacts of dusty projectiles with hard targets lead to extremely flat fragment-ejection angles but rather fast ejecta and, thus, are not likely to produce a significant aerodynamic reaccretion. Impacts into loose dusty bodies cause much steeper ejecta angles and slow ejecta. Although many details of the fragmentation process and the ejection of small dust aggregates are still lacking, many experimental investigations concurrently find that the ejection velocities of the fragments are between <1% and ~10% of the impact velocity (Hartmann 1978; Wurm, Blum & Colwell 2001a; Colwell & Taylor 1999; Colwell 2003; Wurm, Paraskov

& Krauss 2005a; Paraskov, Wurm & Krauss 2007; Colwell et al. 2008), so that the aerodynamic reaccretion is in principle feasible.

7.2.2. Electrostatic re-accretion. The reaccretion efficiency of fragments following a destructive collision among dust aggregates can be enhanced by electrostatic attraction between the larger (surviving) body and the escaping fragments. Based upon laboratory experiments by Poppe, Blum & Henning (2000b), who measured a systematic charge separation in bouncing collisions between a solid target and micrometer-sized dust particles, Blum (2004) suggested that the build-up of a sufficiently strong electric field on the larger dust aggregate can capture oppositely charged ejecta. Similar to the aerodynamic reaccretion, the efficiency of the electrostatic reaccretion depends strongly on the ejecta properties and on the charge separation process. Laboratory studies and numerical simulations of this effect are ongoing (C. Güttler & J. Blum, personal communication).

7.3. The Snow Line

Kretke & Lin (2007) modelled the dynamics of solid bodies around the snow line (i.e., the boundary at which water ice condenses) under the assumption that the condensation of new solid material changes the optical depth and, thus, the depth of the turbulent region of the gas, if the MRI is responsible for the turbulence. Whereas the PPD can be turbulent throughout its thickness inside the snow line, the freshly condensed ice grains just outside the snow line absorb all free charge carriers, owing to their large total surface area, and prevent MRI turbulence close to the midplane. This causes a local maximum in the gas pressure and, thus, a change in the sign of the pressure gradient. Gas at the location of the maximum gas pressure rotates at Keplerian velocity, whereas gas inward (outward) of the maximum pressure region rotates super- (sub-) Keplerian. Due to the differential between gas and dust rotation velocity, dust aggregates in the super- (sub-) Keplerian gas-rotation region drift outward (inward), causing a concentration of the solid bodies close to the pressure maximum. Thus, this effect prevents meter-sized particles from falling into the young star and potentially allows the dust and ice aggregates captured there to grow further due to decreased collision velocities. Whereas the differential in the transverse motion causes high-speed impacts of small dust grains or aggregates into large dust aggregates of up to ~ 50 m s^{-1} throughout the disk, the conditions close to the snow line are different: Owing to the Keplerian rotation of the gas and dust aggregates of all sizes and the absence of radial drift motion, relative velocities can be very moderate. In addition to that, Kretke & Lin (2007) state that dust aggregates at the snow line should be covered with a frost layer. Although frost might not solve the problem of sticking at high collision velocities as mentioned above (Section 7.1.2), it might positively influence the sticking properties at low velocities, as suggested by the experiments of Bridges et al. (1996) and Supulver et al. (1997) (see Section 7.1.2). The concentration of dust and ice aggregates close to the snow line is fed by a continuous source of inward-drifting dust and ice. This concentration enhancement of the solid component can be sustained until the local mass density of the solids exceeds the gas density. Then, the solids cause the gas to drift outward, dragging the dust and ice concentration along. Whether the process discussed by Kretke & Lin (2007) can lead to the formation of planetesimals is still unclear and depends on the kinematics and dynamics inside the ring of concentrated solid material.

7.4. Cumulative Dust Effects and Gravitational Instability

We have seen above that meter-sized dust aggregates drift so rapidly inward that they are either lost to the young star within an extremely short time or have to grow very fast to supermeter sizes

so that their radial drift is slowed. This picture, however, is only true for a laminar gas disk and for a dilute dispersion of dusty bodies within the gaseous accretion disk. Long-lived turbulent eddies can efficiently capture meter-sized bodies and prevent their inward drift (see, e.g., Barge & Sommeria 1995, Klahr & Bodenheimer 2006). The further collisional evolution of such captured bodies has not yet been studied in detail. Relative velocities might be considerably decreased so that collisions can result in sticking, rather than in fragmentation. Due to the continuous supply of new captured bodies, the collision timescale inside such a vortex might become extremely short. However, once the concentration of solid bodies exceeds the mass density of the gas, the feedback of the dust-aggregate motion to the gas motion must be considered.

A similar situation arises in the midplane of the accretion disk, where macroscopic dust aggregates accumulate owing to their vertical sedimentation. The radial drift velocity and the high collision velocities of the solid bodies arise from the shear between the sub-Keplerian gas and the Keplerian rotation of the dust. For high dust concentrations, the feedback from the dusty component to the gas can speed up the gas rotation and lower the radial drift and collision velocities of the dust aggregates. The formation of such a dense dust subdisk owing to the sedimentation of dust aggregates to the midplane of the accretion disk has been widely discussed in the literature (see Dominik et al. 2007 and references therein). The maximum mass density in the dust subdisk strongly depends on the strength of the gas turbulence, which causes vertical diffusion of the dusty bodies. However, even in the absence of external gas turbulence, the dust assemblage cannot become gravitationally unstable, owing to the shear motion between the Keplerian dust and the sub-Keplerian gas rotation (Weidenschilling 1995).

A recent work by Johansen et al. (2007) numerically investigated the cumulative effect of large dust aggregates close to the midplane of a PPD. They assumed MRI turbulence and observed the concentration of decimeter- to meter-sized bodies in transient high-pressure regions. If the dust concentration is high enough, the streaming instability (Youdin & Goodman 2005; Johansen, Henning & Klahr 2006; Johansen & Youdin 2007) causes a further increase in the dust number density. Johansen et al. (2007) observed the formation of gravitationally bound clusters with masses comparable to the largest asteroids within a few orbital timescales. The concentration works best for bodies whose response time to the gas motion is comparable to the orbital timescale. For typical PPD models, this corresponds to aggregate sizes in the meter regime. However, small deviations from the optimal size are tolerable. The work of Johansen et al. (2007) is self-consistent in the sense that it encompasses a three-dimensional numerical solution of the magnetohydrodynamic equations in a differentially rotating gas disk, drag effects between gas and dust in both directions, and gravitational effects between the dust aggregates. However, some uncertainties remain. Before one can state that the processes described by Johansen et al. (2007) are able to really form planetesimals or protoplanets, the following areas must be investigated: (*a*) details of the gas flow inside gravitationally unstable clumps are still to be resolved, (*b*) the role of collisions among the meter-sized dust aggregates inside the clumps is uncertain; questions whether collision-caused fragments can be carried away from the clumps (from the surface or the interior) owing to the high relative velocity of the gravitationally bound dust assemblage and the ambient gas are to be answered, (*c*) the high-velocity headwind that the dust assemblage encounters can lead to sandblasting erosion of the surface of the clump (see Section 5.6), (*d*) how small the dust aggregates inside the clump can become before the gravitational effect breaks down, and what the total mass accreted is if the dust aggregates are much smaller than one meter in size, (*e*) if we assume comets to be the sole survivors of the formation phase of our Solar System, the existence of these bodies shows that at least some material of the young Solar System went through kilometer-sized planetesimals and not directly from meter-sized dust aggregates to protoplanets. Can the model by Johansen et al. (2007) also explain the formation of comets?

7.5. Radial Dependence of Dust Growth

As indicated earlier, the systematic laboratory studies have so far concentrated on refractory materials and gas temperatures of ∼300 K, simulating the conditions in a PPD at ∼1 AU distance from the young solar-type star. Are the conditions at smaller or larger distances more or less favorable for planetesimal formation? Due to the increasing temperature, the dust-to-gas ratio should decrease with decreasing radial distance, as most materials are in the gas phase at higher temperature. In this range, dust aggregates are supposed to get solidified by sintering on short timescales (Poppe 2003). Collisions between sintered dust aggregates are still uninvestigated so that no conclusion on the growth efficiency can be drawn. Eutectic melting between co-existing high-temperature phases could enhance the stickiness of the grains.

Between 1 AU and 2 AU we do not expect any major changes in the collision behavior of the dust aggregates, as recent collision experiments by D. Heißelmann, H. Fraser & J. Blum (unpublished data) at temperatures 140 K < T < 300 K suggest. As mentioned in Sections 7.1.1. and 7.1.2., organic and icy materials might raise the sticking threshold somewhat for radial distances >2 AU, and massive ice-particle condensation at the snow line can locally favor the growth conditions (see Section 7.3.). However, the overall picture that bodies larger than a few centimeters in size experience catastrophic impacts, seems to remain correct.

8. SUMMARY AND OUTLOOK

After an extensive phase of laboratory and theoretical research on the evolution of solid particles and dust aggregates in PPDs, we have gained a much better insight into the collision physics of dust aggregates and their motion within the PPD. We now have a somehow detailed picture of how decimeter-sized dust aggregates form, but lack a self-consistent description of the further evolution of solid bodies to the planetesimal level. Recent work on gravitational instability in turbulent accretion disks shows promising perspectives, but details on the dust evolution within the self-gravitating ensemble of dust aggregates have yet to be clarified before the final verdict can be returned.

SUMMARY POINTS

1. Protoplanetary dust aggregates consisting of dust particles with size s stick in collisions with $v_{st} \lesssim (\frac{1}{s/1\,\mu m})^x$ m s^{-1} velocity, with $x \approx 1$ for 0.1 μm $\lesssim s \lesssim$ 10 μm.

2. The initial growth of dust aggregates proceeds through fractal structures, which are characterized by a mass-size relation of $m \propto s^D$ with $D \lesssim 2$ and a quasi-monodisperse mass distribution. The temporal evolution of the mean aggregate mass in that phase follows a power-law or an exponential growth.

3. For collision energies exceeding the rolling-friction energy of a single grain-grain contact, i.e., for dust aggregates above a certain mass, collisions still result in sticking but in the formation of nonfractal, yet highly porous dust aggregates.

4. The formation of decimeter-sized bodies is feasible with direct hit-and-stick collisions under solar-nebula conditions. Larger bodies can directly form if the constituent dust-particle sizes are much smaller than 1 μm.

5. The timescale for the initial growth is short. Centimeter- to decimeter-sized aggregates should form within only ∼1000 years.

6. Collisions between dust aggregates with collision velocities $v \gtrsim 1$ m s^{-1} do not result in sticking. Compaction and fragmentation are characteristic for high-velocity collisions. However, even macroscopic dust aggregates, which experience collisions with velocities of several tens of meters per second, will be highly porous.

7. Collisions among protoplanetary dust aggregates are complex physical processes, which can result in sticking (hit-and-stick, with compaction, by deep intrusion), bouncing (with or without compaction, with and without mass transfer), erosion, or fragmentation (of the projectile only, of projectile and target, with or without partial sticking). The collisional outcome depends on impact velocity, impact angle, mass of projectile and target, porosity and hardness of projectile and target, radius of curvature of the target surface, size distribution, morphology and material of the dust grains, ambient gas density and gas flow, and the occurrence of impact charging.

8. The direct formation of kilometer-sized planetesimals cannot (yet?) be understood via sticking collisions. Secondary mechanisms, such as the reaccretion of fragments after a destructive collision or cumulative effects of an ensemble of dust aggregates, must be considered.

FUTURE ISSUES

1. The map of aggregate-aggregate collisions (see **Figure 12**) is still far from being complete. More experiments are required to fill the gaps and to establish similar maps for other protoplanetary particle materials (e.g., ices).

2. Self-consistent laboratory experiments are required to study the evolution of single dust aggregates, i.e., the collisional sequence that leads to the growth (and destruction) of individual bodies in PPDs.

3. The influence of dust-aggregate hardening (by impact-compaction or sintering) on their collisional evolution is a potentially important issue that needs to be investigated.

4. Collision experiments should be repeated with aggregates consisting of 100-nm-sized dust particles to prove whether the sticking properties of dust aggregates consisting of smaller grains are different from those consisting of micrometer-sized grains (see **Figure 13**). If the sticking properties of 100-nm-sized grains are very favorable, this might also provide a means to promote the direct collisional formation of planetesimals, considering that the initial size of the dust particles is not very well observationally constrained.

5. Numerical work on the outcome of individual aggregate-aggregate collisions, both for small dust aggregates (by direct molecular-dynamics codes) and for very large dusty objects (by SPH codes), shows promising results and agrees with first benchmark laboratory tests. More work needs to be done here to predict the outcomes of arbitrary protoplanetary dust collisions.

6. The evolution of protoplanetary dust must be modeled in a self-consistent way, including experimental data and model collisions. A realistic treatment of dust morphologies (e.g., fractal dimension and porosity), collisional behavior, charging, sintering, evaporation and condensation, multiparticle phenomena, and multiphase flow should be envisaged.

DISCLOSURE STATEMENT

The authors are not aware of any biases that might be perceived as affecting the objectivity of this review.

LITERATURE CITED

Alexander RD, Armitage PJ. 2007. *MNRAS* 375:500

Alibert Y, Mordasini C, Benz W, Winisdoerffer C. 2005. *Astron. Astrophys.* 434:343

Armitage PJ, Clarke CJ, Palla F. 2003. *MNRAS* 342:1139

Balbus SA, Hawley JF. 1991. *Astrophys. J.* 376:214

Barge P, Sommeria J. 1995. *Astron. Astrophys.* 295:L1

Bell KR, Cassen PM, Wasson JT, Woolum DS. 2000. In *Protostars and Planets IV*, ed. V Mannings, AP Boss, SS Russell, pp. 897–926. Tucson: Univ. Arizona Press

Bizzarro M, Baker JA, Haack H. 2004. *Nature* 431:275–78

Blum J. 2004. *Proc. Astrophysics of Dust, Estes Park*, pp. 369. San Francisco: ASP

Blum J. 2006. *Adv. Phys.* 55:881

Blum J, Bruns S, Rademacher D, Voss A, Willenberg B, Krause M. 2006b. *Phys. Rev. Lett.* 97:230601

Blum J, Münch M. 1993. *Icarus* 106:151

Blum J, Schräpler R. 2004. *Phys. Rev. Lett.* 93:115503

Blum J, Schräpler R, Davidsson BJR, Trigo-Rodríguez JM. 2006a. *Astrophys. J.* 652:1768

Blum J, Wurm G. 2000. *Icarus* 143:138

Blum J, Wurm G, Kempf S, Henning T. 1996. *Icarus* 124:441

Blum J, Wurm G, Kempf S, Poppe T, Klahr H, et al. 2000. *Phys. Rev. Lett.* 85:2426

Blum J, Wurm G, Poppe T, Heim L-O. 1998. *Earth Moon & Planets* 80:285

Blum J, Wurm G, Poppe T, Kempf S, Kozasa T. 2002. *Adv. Space Res.* 29:497

Bottke WF, Nesvorný D, Grimm RE, Morbidelli A, O'Brien DP. 2006. *Nature* 439:821–24

Bouvier J, Alencar SHP, Harries TJ, Johns-Krull CM, Romanova MM. 2007. See Reipurth, Jewitt & Keil 2007, pp. 479–94

Brauer F, Dullemond C, Henning T. 2008. *Astron. Astrophys.* 480:859

Bridges FG, Supulver KD, Lin DNC, Knight R, Zafra M. 1996. *Icarus* 123:422

Brownlee D, Tsou P, Aléon J, Alexander C, Araki T, et al. 2006. *Science* 314:1711

Clarke CJ. 2007. *MNRAS* 376:1350

Colwell JE. 2003. *Icarus* 164:188

Colwell JE, Sture S, Cintala M, Durda D, Hendrix A, et al. 2008. *Icarus*. 195:908

Colwell JE, Taylor M. 1999. *Icarus* 138:241

D'Alessio P, Hartmann L, Calvet N, Franco-Hernández R, Forrest WJ, et al. 2005. *Astrophys. J.* 621:461

Derjaguin BV, Muller VM, Toporov YP. 1975. *J. Coll. Interf. Sci.* 53:314

Dominik C, Blum J, Cuzzi JN, Wurm G. 2007. See Reipurth, Jewitt & Keil 2007, p. 783

Dominik C, Nübold H. 2002. *Icarus* 157:173

Dominik C, Tielens AGGM. 1997. *Astrophys. J.* 480:647

Dullemond CP, Dominik C. 2005. *Astron. Astrophys.* 434:971–86

Dullemond CP, Hollenbach D, Kamp I, D'Alessio P. 2007. See Reipurth, Jewitt & Keil 2007, p. 555

Dullemond CP, Natta A, Testi L. 2006. *Astrophys. J.* 645:L69–72

Dutrey A, Guilloteau S, Ho P. 2007. See Reipurth, Jewitt & Keil 2007, p. 495

Einstein A. 1905. *Ann. Physik.* 322:549

Gail HP. 2004. *Astron. Astrophys.* 413:571

Getman KV, Feigelson ED, Townsley L, Broos P, Garmire G, Tsujimoto M. 2006. *Astrophys. J. Suppl. Ser.* 163:306

Hartmann WK. 1978. *Icarus* 33:50

Hatzes AP, Bridges F, Lin DNC, Sachtjen S. 1991. *Icarus* 89:113

Hayashi C, Nakazawa K, Nakagawa Y. 1985. In *Protostars and Planets II*, ed. DC Black, MS Matthews, pp. 1100. Tucson: Univ. Arizona Press

Heim L-O, Blum J, Preuss M, Butt H-J. 1999. *Phys. Rev. Lett.* 83:3328

Israelachvili JN. 1992. *Intermolecular and Surface Forces*. San Diego: Academic, 450 pp.

Ivlev AV, Morfill GE, Konopka U. 2002. *Phys. Rev. Lett.* 89:195502

Jang-Condell H, Sasselov DD. 2004. *Astrophys. J.* 608:497

Jessberger EK, Stephan T, Rost D, Arndt P, Maetz M, et al. 2001. In *Interplanetary Dust*, ed. E Grün, BAS Gustafson, SF Dermott, H Fechtig, pp. 253. Berlin: Springer-Verlag

Johansen A, Henning T, Klahr H. 2006. *Astrophys. J.* 643:1219

Johansen A, Oishi JS, Low M-MM, Klahr H, Henning T, Youdin A. 2007. *Nature* 448:1022

Johansen A, Youdin A. 2007. *Astrophys. J.* 662:627

Johnson KL, Kendall K, Roberts AD. 1971. *Proc. R. Soc. London A.* 324:301

Kempf S, Pfalzner S, Henning T. 1999. *Icarus* 141:388

Klahr H, Bodenheimer P. 2006. *Astrophys. J.* 639:432

Kouchi A, Kudo T, Nakano H, Arakawa M, Watanabe N, et al. 2002. *Astrophys. J.* 566:L121

Krause M, Blum J. 2004. *Phys. Rev. Lett.* 93:021103

Krauss O, Wurm G, Mousis O, Petit J-M, Horner J, Alibert Y. 2007. *Astron. Astrophys.* 462:977

Kretke KA, Lin DNC. 2007. *Astrophys. J.* 664:L55

Langkowski D, Teiser J, Blum J. 2008. *Astrophys. J.* 675:764

Lauretta DS, McSween HY Jr, eds. 2006. *Meteorites and the Early Solar System II*. Tucson: Univ. Ariz. Press. 942 pp.

Lewis JS. 1997. *Physics and Chemistry of the Solar System*, pp. 70. San Diego: Academic, 591 pp. rev. ed.

Li A, Greenberg JM. 2003. *Proc. NATO Adv. Study Inst. Solid State Astrochem.*, *Erice*, p. 37. Dordrecht: Kluwer Acad.

Malbet F, Lachaume R, Berger J-P, Colavita MM, di Folco E, et al. 2005. *Astron. Astrophys.* 437:627

Meakin P, Donn B, Mulholland G. 1989. *Langmuir* 5:510

Meyer MR, Backman DE, Weinberger AJ, Wyatt MC. 2007. See Reipurth, Jewitt & Keil 2007, p. 573

Najita JR, Carr JS, Glassgold AE, Valenti JA. 2007. See Reipurth, Jewitt & Keil 2007, pp. 507–22

Nübold H, Glassmeier K-H. 2000. *Icarus* 144:149

Nübold H, Poppe T, Rost M, Dominik C, Glassmeier K-H. 2003. *Icarus* 165:195

Nuth JA, Faris J, Wasilewski P, Berg O. 1994. *Icarus* 107:155

Nuth JA, Wilkinson GM. 1995. *Icarus* 117:431

Ormel CW, Spaans M, Tielens AGGM. 2007. *Astron. Astrophys.* 461:215

Papaloizou JCB, Terquem C. 1999. *Astrophys. J.* 521:823

Paraskov GB, Wurm G, Krauss O. 2006. *Astrophys. J.* 648:1219

Paraskov GB, Wurm G, Krauss O. 2007. *Icarus* 191:779

Paszun D, Dominik C. 2006. *Icarus* 182:274

Poppe T. 2003. *Icarus* 164:139

Poppe T, Blum J, Henning T. 2000a. *Astrophys. J.* 533:454

Poppe T, Blum J, Henning T. 2000b. *Astrophys. J.* 533:472

Reißaus P, Waldemarsson T, Blum J, Clément D, Llamas I, et al. 2006. *J. Nanopart. Res.* 8:693

Reipurth B, Jewitt D, Keil K, eds. 2007. *Protostars and Planets V*. Tucson: Univ. Ariz. Press. 1024 pp.

Righter K, Drake MJ, Scott ERD. 2006. See Lauretta & McSween 2006, p. 803.

Rodmann J, Henning T, Chandler CJ, Mundy LG, Wilner DJ. 2006. *Astron. Astrophys.* 446:211

Schäfer C, Speith R, Kley W. 2007. *Astron. Astrophys.* 470:733

Scott ERD, Krot AN. 2005. *Astrophys. J.* 623:571

Sekiya M, Takeda H. 2003. *Earth, Planets, Space* 55:263

Sekiya M, Takeda H. 2005. *Icarus* 176:220

Sirono S-I. 2004. *Icarus* 167:431

Smoluchowski MV. 1916. *Z. Phys.* 17:557

Supulver KD, Bridges FG, Tiscareno S, Lievore J, Lin DNC. 1997. *Icarus* 129:539

Sutherland DN. 1966. *J. Colloid Interface Sci.* 22:300

Takeuchi T, Miyama SM, Lin DNC. 1996. *Astrophys. J.* 460:32

Udry S, Fischer D, Queloz D. 2007. See Reipurth, Jewitt & Keil 2007, p. 685

Vold MJ. 1959. *J. Colloid Interface Sci.* 14:168

Vold MJ. 1963. *J. Colloid Interface Sci.* 18:684

Wada K, Tanaka H, Suyama T, Kimura H, Yamamoto T. 2007. *Astrophys. J.* 661:320

Wadhwa M, Amelin Y, Davis AM, Lugmair GW, Meyer B, et al. 2007. See Reipurth, Jewitt & Keil 2007, p. 835

Wang Z, Chakrabarty D, Kaplan DL. 2006. *Nature* 440:772

Watson PK, Mizes H, Castellanos A, Pérez A. 1997. In *Powders & Grains 9*7, ed. R Behringer, JT Jenkins, p. 109. Rotterdam: Balkema

Weidenschilling SJ. 1977. *MNRAS* 180:57

Weidenschilling SJ. 1980. *Icarus* 44:172

Weidenschilling SJ. 1995. *Icarus* 116:433

Weidenschilling SJ. 1997. *Icarus* 127:290

Weidenschilling SJ, Cuzzi JN. 1993. In *Protostars and Planets III*, ed. EH Levy, JI Lunine, p. 1031. Tucson: Univ. Ariz. Press

Weisberg MK, McCoy TJ, Krot AN. 2006. See Lauretta & McSween 2006, p. 19

Wilner DJ, D'Alessio P, Calvet N, Claussen MJ, Hartmann L. 2005. *Astrophys. J.* 626:L109

Wolszczan A, Frail DA. 1992. *Nature* 355:145

Wood JA. 2000. *Space Sci. Rev.* 92:87

Wurm G, Blum J. 1998. *Icarus* 132:125

Wurm G, Blum J, Colwell JE. 2001a. *Icarus* 151:318

Wurm G, Blum J, Colwell JE. 2001b. *Phys. Rev. E* 64:046301

Wurm G, Paraskov G, Krauss O. 2004. *Astrophys. J.* 606:983

Wurm G, Paraskov G, Krauss O. 2005a. *Phys. Rev. E* 71:021304

Wurm G, Paraskov G, Krauss O. 2005b. *Icarus* 178:253

Wurm G, Schnaiter M. 2002. *Astrophys. J.* 567:370

Wyatt MC, Dent WRF, Greaves JS. 2003. *MNRAS* 342:876

Youdin AN, Goodman J. 2005. *Astrophys. J.* 620:459

Zolensky M, Zega T, Yano H, Wirick S, Westphal A, et al. 2006. *Science* 314:1735

Contents

Indexes

Errata

An online log of corrections to *Annual Review of Astronomy and Astrophysics* articles may
be found at http://astro.annualreviews.org/errata.shtml